International Journal of Pharmaceutics: X 9 (2025) 100341

Contents lists available at ScienceDirect

International Journal of Pharmaceutics: X

journal homepage: www.sciencedirect.com/journal/international-journal-of-pharmaceutics-x

Development, characterization, and *in vitro* evaluation of poly(ethylene oxide)-*block*-poly(ε-caprolactone)-α-tocopheryl succinate micelles as a novel nanocarrier for rapamycin delivery

Ziyad Binkhathlan [a,b,*], Abdullah K. Alshememry [a,b,*], Ahmad M. Balkhair [a,1], Raisuddin Ali [a,b], Sulaiman S. Alhudaithi [a,b], Saad Alobid [c], Wajhul Qamar [c], Alhassan H. Aodah [d], Mohammad Reza Vakili [e], Afsaneh Lavasanifar [e,f]

[a] *Department of Pharmaceutics, College of Pharmacy, King Saud University, P.O. Box 2457, Riyadh 11451, Saudi Arabia*
[b] *Nanobiotechnology Research Unit, College of Pharmacy, King Saud University, P.O. Box 2457, Riyadh 11451, Saudi Arabia*
[c] *Department of Pharmacology and Toxicology, College of Pharmacy, King Saud University, P.O. Box 2457, Riyadh 11451, Saudi Arabia*
[d] *Advanced Diagnostics and Therapeutics Institute, Health Sector, King Abdulaziz City for Science and Technology (KACST), 11442 Riyadh, Saudi Arabia*
[e] *Faculty of Pharmacy and Pharmaceutical Sciences, University of Alberta, Edmonton, Alberta T6G 2H7, Canada*
[f] *Department of Chemical and Material Engineering, University of Alberta, Edmonton, Alberta T6G 2V4, Canada*

ARTICLE INFO

Keywords:
Alpha-tocopheryl succinate
Block copolymer
In vitro cytotoxicity
In vitro release
Polymeric micelles
Rapamycin

ABSTRACT

Rapamycin holds significant therapeutic potential for various diseases; however, its clinical application is limited by several formulation challenges, primarily its extremely low aqueous solubility (2.6 μg/mL). To address this, nanoparticle-based delivery systems have emerged as a promising strategy to enhance solubility and enable sustained drug release. Currently, Fyarro® (Aadi Bioscience, Inc.), an albumin-bound nanoparticle formulation, is the only FDA-approved injectable rapamycin product. In this study, we aimed to develop and evaluate novel poly(ethylene oxide)-*block*-poly(ε-caprolactone)-α-tocopheryl succinate (PEO-*b*-PCL-α-TS) micelles and assess their potential as a delivery system for rapamycin. PEO-*b*-PCL copolymers with varying PCL/PEO ratios were prepared *via* ring-opening polymerization and modified by α-TS conjugation, as confirmed by ^{1}H NMR, GPC, XRD, DSC analyses. The optimum rapamycin-loaded micelles (PEO_{2000}-*b*-PCL_{4000}-α-TS) exhibited nano-sized particles (< 22 nm) with a narrow polydispersity index (<0.29), high drug encapsulation efficiency (≥92 %), and enhanced solubility (>1.3 mg/mL). Stability studies demonstrated that encapsulation protected rapamycin from degradation, maintaining over 90 % drug retention for three months at 4 °C, while *in vitro* release studies showed sustained release, with 50 % of rapamycin released from PEO_{2000}-*b*-PCL_{4000}-α-TS micelles over 72 h. *In vitro* cytotoxicity assays revealed anticancer activity against lung carcinoma epithelial cells (A549), and the human colon adenocarcinoma cell line (HCT116). Minimal toxicity (≥70 % viability) was observed in normal human fibroblast cells (HFF1). These results point to the potential of PEO-*b*-PCL-α-TS micelles as a promising nanocarrier system, offering improved rapamycin solubility, enhanced stability, sustained release, and effective anticancer activity.

1. Introduction

Many newly discovered chemical compounds have a problem of low solubility in water, with more than 40 % of active ingredients being hydrophobic. This poses difficulties in formulating them for parenteral administration and leads to delays in bringing these drugs to market (Lipinski, 2002). In the case of anticancer drugs, the majority suffer from issues like low bioavailability, instability in biological environments, challenges in achieving effective concentrations at the site of action, and the emergence of multidrug resistance (Chidambaram et al., 2011).

Rapamycin, also known as sirolimus, is a compound derived from *Streptomyces hygroscopicus*, belonging to the polyketide macrolide family

* Corresponding authors at: Department of Pharmaceutics, College of Pharmacy, King Saud University, P.O. Box 2457, Riyadh 11451, Saudi Arabia.
E-mail addresses: zbinkhathlan@ksu.edu.sa (Z. Binkhathlan), aalshememry@ksu.edu.sa (A.K. Alshememry), ambalkhair@iau.edu.sa (A.M. Balkhair).
[1] Present address: Department of Nano-Medicine Research, Institute for Research and Medical Consultations (IRMC), *Imam* Abdulrahman Bin Faisal University, P. O. Box 1982, Dammam 31,441, Saudi Arabia.

https://doi.org/10.1016/j.ijpx.2025.100341
Received 8 February 2025; Received in revised form 23 May 2025; Accepted 24 May 2025
Available online 29 May 2025

(Sehgal et al., 1975). It interacts with FK505 binding protein 12 (FK505–12) to form a complex that inhibits the activity of mTOR kinase. As a result, signaling pathways dependent on interleukin-2 (IL-2) receptor and CD28 are blocked (Dowling et al., 2010). Preclinical and clinical studies have shown that rapamycin is effective in treating various diseases related to the immune system (*e.g.*, autoimmune diseases and graft rejection) (Hartford and Ratain, 2007), neurodegenerative disorders (*e.g.*, Alzheimer's disease) (Li et al., 2014), metabolic disorders (*e.g.*, obesity and diabetes) (Chang et al., 2009; Krebs et al., 2007; Ong et al., 2016; Um et al., 2004), and several types of cancer including breast cancer, renal cell carcinoma, colon cancer, lung cancer, and lymphoma (Law, 2005; Li et al., 2014).

Rapamycin holds significant potential for treating various health conditions; however, its clinical application faces several challenges. These include its limited water solubility (2.6 μg/mL) (Simamora et al., 2001), susceptibility to gastric acid degradation (Kim et al., 2013), and being a substrate for intestinal and hepatic cytochrome P450 enzymes as well as the P-glycoprotein efflux pump (Lampen et al., 1998). These factors contribute to its low and variable oral bioavailability, estimated to be approximately 14 % with the oral solution (MacDonald et al., 2000). Commercially, rapamycin is available under the trade name Rapamune® as an oral solution (1 mg/mL; 60 mL) and tablets (0.5, 1, and 2 mg).

These drawbacks highlight the need for the development of pharmaceutical nanotechnology in order to improve the delivery of rapamycin, making it more accurate and effective. One promising approach involves incorporating rapamycin into nanoparticle systems, which can enhance its solubility and enable sustained drug release (Haeri et al., 2018). Among the efforts in this field, ABI-009 (Fyarro®, Aadi Bioscience, Inc.) is the first and only FDA-approved rapamycin injectable product. It is an albumin-bound nanoparticle formulation (~100 nm) developed with nab®-technology, which was approved to treat adult patients with locally advanced unresectable or metastatic malignant perivascular epithelioid cell tumors (PEComa). Preclinical studies demonstrated that Fyarro® achieves significantly improved tumor growth inhibition, higher drug accumulation within tumors, and more effective suppression of the mTOR target phospho-S6 compared to oral inhibitors (Wagner et al., 2021). It is currently undergoing several clinical trials for the treatment of other types of malignancies and conditions.

Polymeric micelles are self-assembled nanoparticles consisting of a core and shell structure, formed from amphiphilic block copolymers. Polymeric micelles have attracted considerable attention, primarily due to their low critical micelle concentration (CMC), and relatively rigid core structure. These characteristics impart higher thermodynamic stability to the formulation in physiological solutions, a slower rate of dissociation. As a result, the drug is retained for a longer time, allowing for greater accumulation at the tumor site by evading the reticuloendothelial system that has been made possible due to small size and stealth properties of the most commonly used polymeric micellar structures (Aliabadi and Lavasanifar, 2006).

One of the widely investigated type of block copolymer micelles are those composed of methoxy poly(ethylene oxide)-*block*-poly(ε-caprolactone) (PEO-*b*-PCL) (Grossen et al., 2017). These micelles have gained prominence due to the biocompatibility of PEO, which imparts "stealth" behavior to the formulation (Lin et al., 2005; Otsuka et al., 2003). On the other hand, PCL, with its poly(ester) core, is considered safe for human application due to its susceptibility to hydrolysis and conversion to biocompatible building blocks (Grossen et al., 2017). PEO-*b*-PCL micelles have been extensively studied as long-circulating drug carriers that passively accumulate in tumor tissues, taking advantage of the enhanced permeability and retention effect (Lin et al., 2005; Otsuka et al., 2003). Additionally, these micelles enhance the solubilization of hydrophobic drugs (Grossen et al., 2017).

D–α–tocopheryl succinate (α-TS) is a succinic acid derivative of α–tocopherol (vitamin E). Studies in the last four decades have shown that α-TS possess anticancer activity both *in vitro* and *in vivo* (Prasad et al., 2003). The most intriguing aspect of this α-TS effect is its selectivity toward cancer cells (*i.e.*, does not affect the proliferation of most normal cells). Indeed, numerous studies have shown that α-TS enhances the growth-inhibitory effects of ionizing radiation, chemotherapeutic agents, hyperthermia, and some biological response modifiers selectively on cancer cells, but not on normal cells (Neuzil et al., 2001; Prasad and Edwards-Prasad, 1982; Prasad et al., 2003; Sylvester, 2007; Turley et al., 1997; Turley et al., 1995; Weber et al., 2002; Yu et al., 1997).

In this study, novel block copolymers consisting of PEO-*b*-PCL-α-TS were synthesized and comprehensively characterized using various analytical techniques. These copolymers were utilized to prepare micelles, which were systematically evaluated for their ability to encapsulate rapamycin, enhance its aqueous solubility and stability, provide sustained drug release, and selectively affect the viability of cancer cells with minimal toxicity to normal cells.

2. Materials and methods

2.1. Materials

Methoxy poly(ethylene oxide) (2 kDa and 5 kDa), ε-caprolactone, α-TS, oxalyl chloride (reagent grade, 98 %), triethylamine (TEA) (≥99 %), diethyl ether (reagent grade), dichloromethane (DCM; reagent grade), and dimethyl sulfoxide (DMSO; HPLC grade) were obtained from Sigma Aldrich Co., (St. Louis, MO, USA). Rapamycin was obtained from PKC Pharmaceuticals Inc. (Woburn, MA, USA). Deuterated chloroform ($CDCl_3$, 99.8 %) was purchased from Cambridge Isotope Laboratories Inc. (Tewksbury, MA, USA). Human breast cancer cells (MCF-7) were purchased from the American Type Culture Collection (Manassas, VA, USA). Acetone and acetonitrile (HPLC grade) were acquired from BDH Laboratory Supplies (BDH Chemicals, Poole, UK). Chloroform (HPLC grade) was purchased from Acros Organics (Morris Plains, NJ, USA).

2.2. Methods

2.2.1. Synthesis of PEO-b-PCL and PEO-b-PCL-α-TS copolymers

PEO-*b*-PCL copolymers were synthesized as previously described (Ali et al., 2017; Aliabadi et al., 2005). Methoxy PEO with molecular weight of 2000 or 5000 Da to synthesize PEO_{2000}-*b*-PCL and PEO_{5000}-*b*-PCL copolymers with PEO:PCL molar ratios of 1:1, 1:2, and 1:3. The corresponding PEO-*b*-PCL-α-TS derivatives were synthesized in two major steps (Fig. 1). The first step was the chlorination of α-TS to synthesize α-tocopheryl succinyl chloride. α-TS (1 mmol) was dissolved in anhydrous DCM in a round-bottom flask. While the solution was cooled down by an ice bath, oxalyl chloride (1.2 mmol) was added to the flask in a dropwise manner. The reaction solution was stirred at room temperature for 4–6 h at room temperature. DCM was removed by vacuum and the reaction mixture was washed with anhydrous hexane. The chlorinated product was dissolved in a fresh anhydrous DCM. The flask was sealed with a rubber septum under argon (Ar) inert atmosphere. The flask was then cooled down using an ice bath. Next, PEO-*b*-PCL copolymer (1 mmol) was dissolved in anhydrous DCM and then added slowly to the reaction mixture (using a syringe and needle) while stirring. Purified TEA (2 mmol) was then added to the reaction mixture, in a dropwise manner. The mixture was stirred at room temperature for 48–72 h. The DCM was evaporated under vacuum. The residue (product) was reconstituted with a minimum amount of DMSO and then dialyzed against DMSO using a dialysis bag (MWCO ~3.5 kDa) for 24 h. The DMSO was then discarded, and the product was dialyzed against distilled water for ~6 h, during which the water was replaced every 1 h. Thereafter, the crude product was freeze-dried for ~48 h. Finally, the freeze-dried product (PEO-*b*-PCL-α-TS) was purified by dissolving it in DCM and precipitating in hexane, which was then dried in a vacuum oven at ~40 °C for 1–2 days. The purification process was repeated 2–3 times (as required) to ensure the complete removal of unreacted α-TS, which was

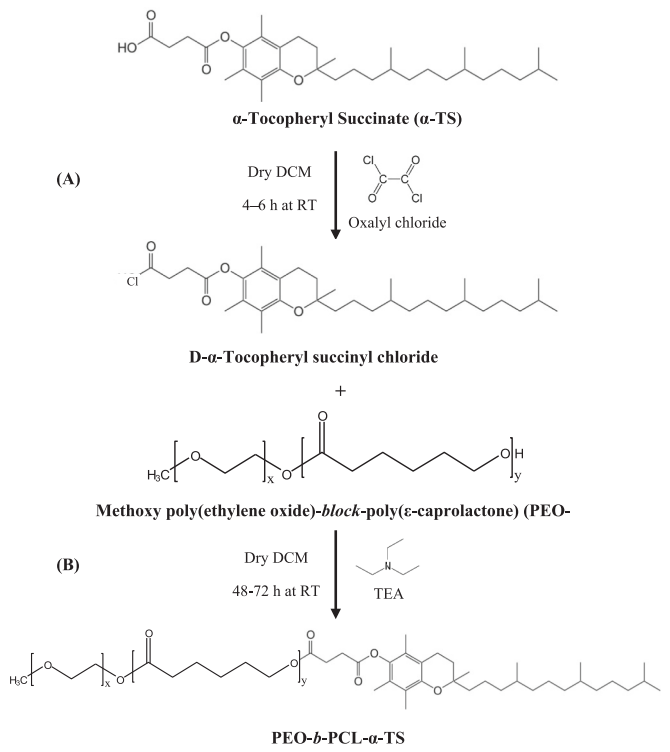

Fig. 1. Synthetic scheme for PEO-*b*-PCL-α-TS copolymers (x = 45 or 114; y = 18, 35, or 52 for PEO_{45}-based copolymers; and 44, 88, or 131 for PEO_{114}-based copolymers). RT: room temperature. DCM: Dichloromethane.

confirmed by ^{1}H NMR.

2.2.2. Characterization of PEO-b-PCL and PEO-b-PCL-α-TS copolymers

2.2.2.1. NMR spectroscopy. Proton nuclear magnetic resonance spectroscopy (^{1}H NMR) at 500 MHz (Bruker Ultrashield 500.133 MHz spectrometer) of PEO-*b*-PCL in deuterated chloroform ($CDCl_3$) was used to assess the conversion of ε-caprolactone to PCL. It was also used to determine the number average molecular weight of the PEO-*b*-PCL copolymers and to assess the conjugation efficiency of α-TS moiety to the terminal hydroxy group of PCL segment [22]. Topspin software was used for baseline correction, calibration, and data processing. To determine the degree of polymerization of ε-CL in each copolymer, the peak intensity ratio of the methylene protons in the PCL segment (-O-CH_2) and the methylene protons in the PEG segment (-O-CH_2-CH_2) at chemical shifts of 4.08 ppm and 3.66 ppm, respectively, were analyzed in the ^{1}H NMR spectra. To determine the conjugation efficiency (%) of α-TS to PEO-*b*-PCL copolymers, the peak intensity ratio of the four methyl groups (-CH_3) on the aliphatic hydrocarbon side chain of α-TS to the methylene protons in the PCL segment (-O-CH_2) at chemical shifts of 0.88 ppm and 4.08 ppm, respectively, were analyzed in the ^{1}H NMR spectra.

2.2.2.2. Gel permeation chromatography (GPC). The number-averaged molecular weights, weight-averaged molecular weights, and molecular weight distributions (dispersity) of the synthesized copolymers were determined by gel permeation chromatography (GPC) (Viscotek TDA 305–040 Triple Detector Array, Viscotek Corp., Houston, TX, USA). 100 µL of polymer stock solutions (15 mg/mL in THF) were injected into a PLgel 5 µm MIXED-D, 7.5 × 300 mm (Agilent Technologies Inc., Santa Clara, CA, USA). The mobile phase, THF, was delivered at a flow rate of 1 mL/min. A calibration curve was created using polystyrene standards. The analysis was conducted at 35 °C. The data acquisition and processing were conducted using OmniSEC™ software from Malvern, USA. Before running the samples, GPC calibration was performed using EasiVial PS-M standards from Varian, USA.

2.2.2.3. X-ray diffraction (XRD). A Rigaku MiniFlex benchtop XRD instrument (Tokyo, Japan) was used to perform X-Ray Diffraction (XRD) analysis to assess changes in the crystallinity. Briefly, an appropriate amount of sample was transferred to the sample holder and leveled to a uniform surface using a glass slide. The sample holder was then placed on the MiniFlex XRD stage, and diffractograms were recorded over a 2θ range of 3° to 50° at a scanning rate of 1°/min. Instrument control and data processing were carried out using Rigaku SmartLab Studio II software.

2.2.2.4. Differential scanning calorimetry (DSC). The thermal behavior of the samples was analyzed using a Differential Scanning Calorimeter (DSC 3+; Mettler Toledo, Worthington, OH, USA) at a heating rate of 10 °C/min over a temperature range of 25° to 200 °C. A dry nitrogen purge at a flow rate of 50 mL/min was maintained throughout the analysis. Instrument control and data processing were performed using Mettler Toledo STARe software.

2.2.3. Preparation and characterization of PEO-b-PCL-α-TS nanocarriers

PEO-*b*-PCL and PEO-*b*-PCL-α-TS micelles were prepared using a co-solvent evaporation method [22]. Briefly, copolymer with or without drug were dissolved in acetone, followed by dropwise addition of the mixture to distilled water. The mixture was left stirring overnight at room temperature, and then a vacuum was applied to ensure the complete removal of the organic solvent. The colloidal solutions were then centrifuged to remove any drug or copolymer precipitate.

The mean diameter and size distribution of the drug-free and rapamycin-loaded micelles were estimated by a dynamic light scattering (DLS) technique using a Malvern Zetasizer™ Nano ZS analyzer (Malvern Instruments Ltd., UK) [22].

CMC was also estimated by the DLS technique [24]. To obtain various concentrations of a block copolymer, successive two-fold serial dilutions were carried out using distilled water. The intensity of the scattered light from the prepared micelles in the diluted samples was measured until it matched the intensity of light scattering observed in water. The Zetasizer™ Nano ZS analyzer from Malvern Instruments Ltd., UK, was utilized to measure the light scattering intensity in kilo counts per second (kcps) for each concentration of the block copolymers. This measurement principle relies on the fact that the kcps readings remain constant below the CMC, which abruptly increase at concentrations equal to the CMC. All measurements were conducted at a temperature of 25 °C [24].

The level of drug encapsulation was determined in the supernatant using the HPLC assay described below [23]. Drug loading (DL%) and encapsulation efficiency (EE%) were determined using the following equations:

$$\mathrm{DL\%(w/w)} = \frac{\text{Amount of loaded drug (mg)}}{\text{Amount of polymer (mg)} + \text{Amount of loaded drug (mg)}} \times 100$$

$$\text{EE}\ (\%) = \frac{\text{Amount of loaded drug (mg)}}{\text{Amount of drug added (mg)}} \times 100$$

Morphology of the micelles was characterized by transmission electron microscopy (TEM). The samples were diluted 20 times using water. Then, 3 µL of diluted sample was added to the a 300-mesh copper grid containing Carbon type-B support film (Ted Pella, Inc., Redding, CA, USA) and allowed to air dry for 15 min. The excess water was removed using thin strips of Whatman filter paper. Then, 3 µL of 1 % phosphotungstic acid solution (negative stain) was added to the same grid and allowed to air dry for 10 min. Again, the excess liquid was removed with a strip of filter paper. The grids were then left to dry in a desiccator for 24 h. The dried grids were then observed under the JEM-1011 TEM (JEOL, Japan) operating at an accelerating voltage of 80 kV. Images were recorded using bottom-mounted 5.3 Megapixel TEM CCD camera TENGRA (Olympus, Germany) and processed with iTEM (Olympus Soft Imaging Solutions GmbH, Germany) software.

2.2.4. *In vitro drug release from PEO-b-PCL-α-TS nanocarriers*

The *in vitro* release of rapamycin from the micelles was investigated using a dialysis bag method. Briefly, 1 mL (containing 0.5 mg of drug) of PEO-*b*-PCL-α-TS or PEO-*b*-PCL micellar formulation were loaded into dialysis bags and immersed in 80 mL of receiving phase. The receiving phase was an aqueous solution prepared by mixing 25.9 vol% of 0.78 M N,N-diethylnicotinamide (DENA) solution, which served as a hydrotropic agent, 10 vol% of ethanol, 10 vol% Tween 20 (20 %), 44.1 vol% Milli-Q water, and 10 vol% 1× PBS (pH 7.4) (Othman et al., 2016). The study was conducted at 37 °C with occasional shaking (50 rpm). At predetermined time intervals (0.25, 0.5, 1, 2, 3, 5, 12, 24, 48, and 72 h), samples were withdrawn from the dialysate and replaced with an equal volume of fresh medium. The drug content in each sample was determined using the HPLC assay method described below.

To better simulate *in vivo* physiologic conditions, the *in vitro* release of the drug from micelles was investigated in the presence of bovine serum albumin (BSA) (40 mg/mL). The release experiment was based on the methodology described by Forrest et al. (Forrest et al., 2006), with minor modifications. Briefly, 3 mL of micelle solutions containing 700 µg of rapamycin were added inside dialysis bags (MWCO = 12–14 kDa) along with BSA. Each bag was then immersed into 200 mL of deionized water and incubated at 37 °C using a shaking water bath (50 rpm).

At predetermined time intervals (0.25, 0.5, 1, 2, 4, 6, 9, 12, 24, 48, and 72 h), 100 uL samples were collected from inside the bag. To maintain a consistent volume, each sample withdrawal was followed by the addition of an equal volume of deionized water. For comparison, the release profile of free rapamycin was also studied under the same experimental conditions. For the control, 2100 µg of rapamycin was initially dissolved in 100 µL of methanol, then diluted with 8.9 mL of deionized water and sonicated. Following sonication, 360 mg of BSA was added to the mixture and sonicated again to ensure full dissolution. A 3-mL aliquot of this solution was loaded into dialysis bags. To maintain sink conditions, the external release medium was changed frequently (every 4 h during the first 12 h of the study and less frequently afterwards).

For drug quantification, the collected samples (100 µL) were diluted with 900 µL of acetonitrile, vortex-mixed, and then centrifuged at 13,500 rpm for 10 min to precipitate BSA. The supernatant was then analyzed using an ultra-performance liquid chromatography (UPLC)-UV following the conditions previously established by Forrest et al. (Forrest et al., 2006). All the *in vitro* release studies were performed in triplicate.

2.2.5. *Determination of rapamycin concentration using an HPLC-UV Assay method*

Rapamycin levels were determined using high-performance liquid chromatography (HPLC)-UV. The HPLC system (Waters™ 1500 series controller, USA) is equipped with a wavelength detector (Waters™ 2489 a Dual UV/Vis Detector, USA), pump (Waters™ 1525 a Binary HPLC Pump, USA), and an automated sampling system (Waters™ 2707 Plus Autosampler, USA). The HPLC system was monitored by "Breeze (Waters™)" software. Rapamycin was analyzed by injecting 20 µL into a C_{18} column (Macherey-Nagel, 4.6 µm × 150 mm, 10 µm particle size). The column temperature was kept at 60 °C. Acetonitrile and Milli-Q® water (pH adjusted to 3 by orthophosphoric acid) at a ratio of 75:25 was used as a mobile phase. The flow rate of the mobile phase was 1 mL/min, and detection was carried out at 277 nm.

2.2.6. *In vitro micelle stability and drug leakage studies*

To evaluate the stability of the developed rapamycin-loaded micelles, changes in micelle size, PDI, and drug leakage were monitored throughout the storage period. Freshly prepared 1 mL samples of micelle dispersions were stored under two conditions: 4 °C and room temperature (25 °C), for up to 6 months. The samples were analyzed for changes in micelle size and PDI using DLS, and drug content (%) using HPLC. Measurements were taken daily during the first week, and subsequently at 0.5, 1, 2, 3, and 6 months of storage.

2.2.7. *In vitro cytotoxicity study*

Rapamycin activity on the human fibroblast cell line (HFF1), the human lung carcinoma epithelial cells (A549), and the human colon adenocarcinoma cell line (HCT116) was determined by measuring the capacity of viable cells to reduce enzymes that convert 3-[4,5-dimethylthiazol-2-yl]-2,5-diphenyltetrazolium bromide (MTT) to colored formazan crystals (van Meerloo et al., 2011). The cells were plated in 96-well plates at a density of 1–1.5 × 10^4 and cultured overnight in 100 µL of DMEM supplemented with 10 % FBS and 1 % antibiotics at 37 °C and 5 % CO_2. Cells were treated with different concentrations of rapamycin (0.78, 1.56, 3.12, 6.25, 12.5, 25, 50, and 100 µM) for 24 and 72 h. Following the removal of the media, cells were incubated with 0.5 mg/mL MTT for 3 h. The color intensity in each well was measured by optical density at a wavelength of 490 nm using an EL 312 96-well microplate reader (Bio-Tek Instruments Inc., Winooski, VT, USA). Cell viability percentages were calculated relative to control wells, which were designated as 100 % viable cells. IC_{50} values were determined using non-linear fit of normalized data (log inhibitor *versus* normalized response). The different treatment groups included rapamycin-loaded PEO-*b*-PCL-α-TS micelles, unloaded PEO-*b*-PCL-α-TS nanocarriers, rapamycin-loaded PEO-*b*-PCL micelles, and unloaded PEO-*b*-PCL micelles.

2.2.8. *Data and statistical analyses*

The data were presented as the mean ± standard deviation (SD). Depending on the number of groups being compared, statistical significance was assessed using either Student's *t*-test or one-way analysis of variance (ANOVA). A p-value <0.05 was considered statistically significant.

3. Results

3.1. *Synthesis and characterization of PEO-b-PCL and PEO-b-PCL-α-TS copolymers*

Twelve copolymers were successfully synthesized and characterized (Table 1). Various analytical methods including ^{1}H NMR, GPC, XRD, and DSC were used to characterize the copolymers.

3.2. *NMR spectroscopy*

Fig. 2 displays typical ^{1}H NMR spectra for α-TS, PEO-*b*-PCL, and a representative PEO-*b*-PCL-α-TS copolymer. The α-TS spectrum (Fig. 2a) reveals the characteristic signals corresponding to the tocopheryl succinate structure. The signals around $\delta = 0.86$–0.90 ppm are attributed to the four methyl groups in the hydrocarbon (isoprenoid) tail, and those around δ = 1.16–1.55 ppm correspond to the methylene protons

Table 1
Characteristics of the synthesized PEO-*b*-PCL and PEO-*b*-PCL-α-TS copolymers and their unloaded self-assembled micelles.

Copolymer [a]	Theoretical MW (g/mol)	M_n (g/mol) [b]	M_n (g/mol) [c]	Đ [d]	Micelle size [e] (nm)	Polydispersity [e]	CMC [e] (μM)
PEO_{2000}-*b*-PCL_{2000}	4000	4080	5030	1.452	$31.0 \pm 1.36^{g,h}$	0.112 ± 0.026	$62.51 \pm 0.44^{g,h}$
PEO_{2000}-*b*-PCL_{2000}–α-TS	4530	4620	7380	1.465	$24.5 \pm 2.04^{*f,g,h}$	0.132 ± 0.028	$50.40 \pm 0.92^{*f,g,h}$
PEO_{2000}-*b*-PCL_{4000}	6000	6180	7040	1.655	40.3 ± 0.93^{h}	0.101 ± 0.003	$36.09 \pm 1.75^{f,h}$
PEO_{2000}-*b*-PCL_{4000}–α-TS	6530	6770	9570	1.658	$27.9 \pm 1.20^{*h}$	0.159 ± 0.006	$30.96 \pm 1.68^{*f,h}$
PEO_{2000}-*b*-PCL_{6000}	8000	7940	8960	1.758	$45.9 \pm 2.09^{f,g}$	0.183 ± 0.059	$18.34 \pm 0.64^{f,g}$
PEO_{2000}-*b*-PCL_{6000}–α-TS	8530	9030	11,120	1.729	$36.3 \pm 4.47^{*}$	0.191 ± 0.052	$25.18 \pm 0.84^{*f,g}$
PEO_{5000}-*b*-PCL_{5000}	10,000	9880	8840	1.414	48.0 ± 0.74^{k}	0.145 ± 0.30	$27.17 \pm 2.29^{j,k}$
PEO_{5000}-*b*-PCL_{5000}–α-TS	10,530	10,100	10,670	1.347	$54.0 \pm 1.04^{*}$	0.154 ± 0.023	$24.81 \pm 2.63^{j,k}$
PEO_{5000}-*b*-PCL_{10000}	15,000	14,800	11,660	1.634	52.5 ± 1.62	0.151 ± 0.078	$16.68 \pm 2.43^{i,k}$
PEO_{5000}-*b*-PCL_{10000}–α-TS	15,530	15,130	13,670	1.539	53.1 ± 2.08	0.180 ± 0.022	$13.52 \pm 1.52^{i,k}$
PEO_{5000}-*b*-PCL_{15000}	20,000	19,790	14,570	1.753	56.0 ± 4.76	0.140 ± 0.025	$8.56 \pm 0.55^{i,j}$
PEO_{5000}-*b*-PCL_{15000}–α-TS	20,530	21,400	16,930	1.655	$66.9 \pm 3.72^{*i,j}$	0.197 ± 0.016	$7.77 \pm 0.94^{i,j}$

[a] The number shown as a subscript indicates the molecular weight of each block determined by ^{1}H NMR. [b] Number-average molecular weight measured by ^{1}H NMR. [c] Number-average molecular weight measured by GPC. [d] Dispersity (M_w/M_n) determined by GPC. [e] Estimated by the DLS technique. * Significantly different form the unmodified PEO-*b*-PCL counterpart ($p < 0.05$; Student's *t*-test). [f] Differences were considered significant compared to PEO_{2000}-*b*-PCL_{2000} ($p < 0.05$; one-way ANOVA followed by Tukey's multiple comparisons test). [g] Differences were considered significant compared to PEO_{2000}-*b*-PCL_{4000} ($p < 0.05$; one-way ANOVA followed by Tukey's multiple comparisons test). [h] Differences were considered significant compared to PEO_{2000}-*b*-PCL_{6000} ($p < 0.05$; one-way ANOVA followed by Tukey's multiple comparisons test). [i] Differences were considered significant compared to PEO_{5000}-*b*-PCL_{5000} ($p < 0.05$; one-way ANOVA followed by Tukey's multiple comparisons test). [j] Differences were considered significant compared to PEO_{5000}-*b*-PCL_{10000} ($p < 0.05$; one-way ANOVA followed by Tukey's multiple comparisons test). [k] Differences were considered significant compared to PEO_{5000}-*b*-PCL_{15000} ($p < 0.05$; one-way ANOVA followed by Tukey's multiple comparisons test).

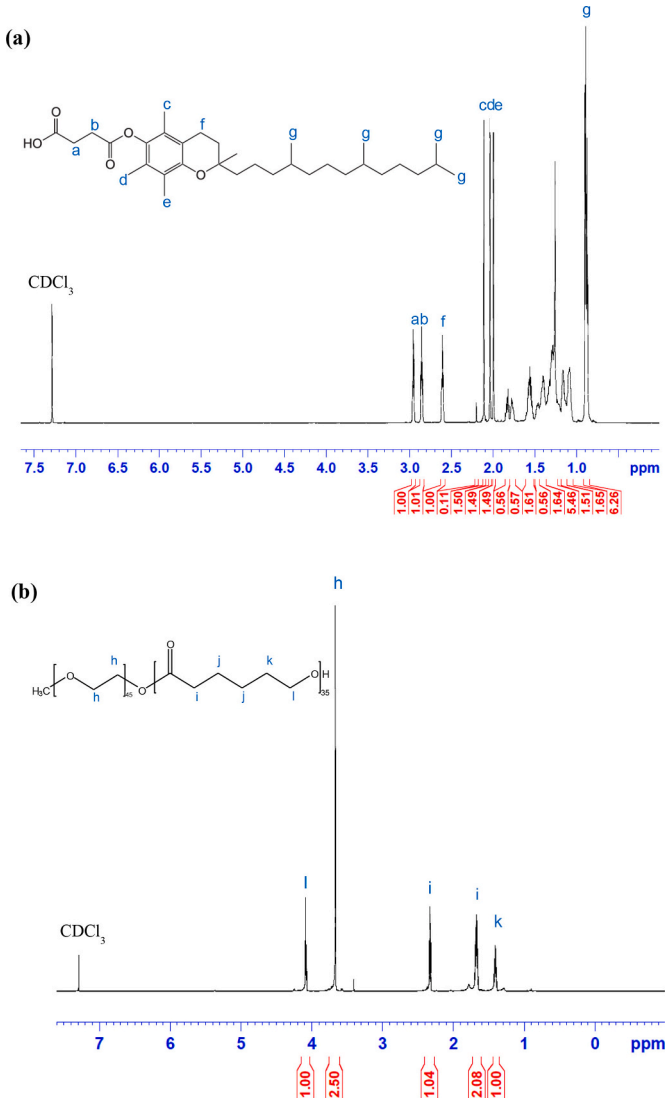

Fig. 2. Representative ^{1}H NMR spectra of α-TS (a), PEO_{2000}-*b*-PCL_{4000} (b), and PEO_{2000}-*b*-PCL_{4000}-α-TS (c).

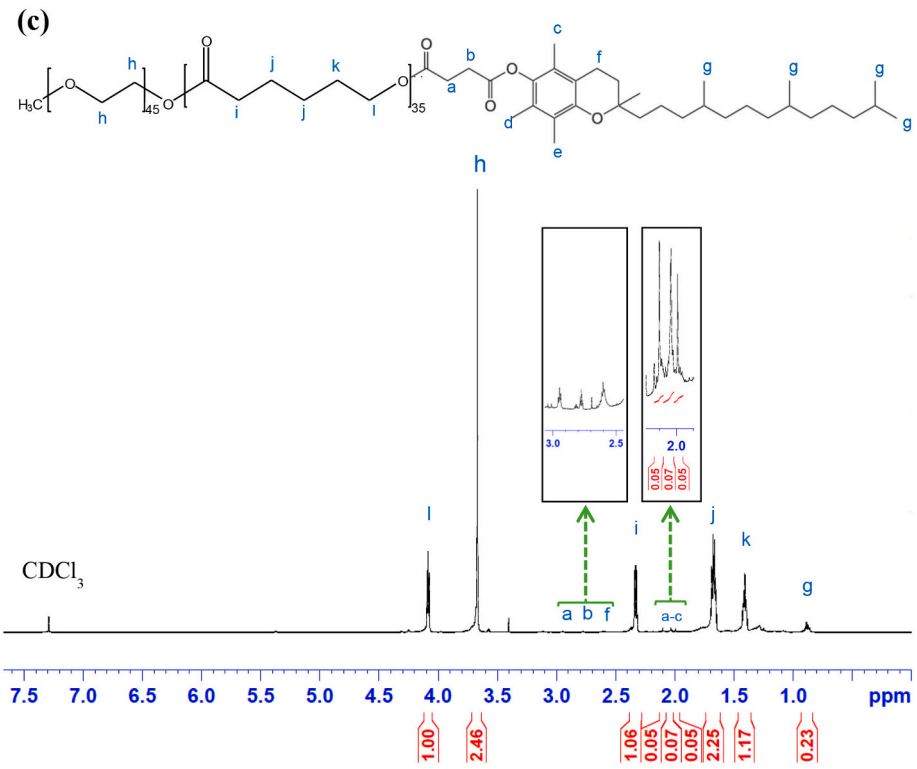

Fig. 2. (*continued*).

adjacent to these methyl groups. The multiplet observed at around δ = 2.00–2.20 ppm corresponds to the three methyl groups at the 5, 7, and 8 positions of the chromanol ring. The peaks observed at the δ = 2.60–2.97 ppm corresponds to the protons of the succinate ester group.

Fig. 2b shows a representative PEO-*b*-PCL copolymer (PEO_{2000}-*b*-PCL_{4000}). The strong peak at δ = 3.66 ppm is assigned to the methylene protons (-CH_2CH_2O-) of the PEO block, while the peaks around δ = 4.08 ppm correspond to the methylene protons adjacent to the ester group in the PCL block (-O-CH_2-). The methylene groups further down the PCL chain are represented by the peaks around δ = 1.38–1.68 ppm, indicating the presence of the aliphatic backbone of PCL. Analyzing the intensity ratio between the peaks at δ = 4.08 ppm and 3.66 ppm in the ^{1}H NMR data allowed determination of molecular weight and composition of the synthesized copolymers (Table 1). Comparison of the ^{1}H NMR results with theoretical values confirms the successful synthesis of PEO-*b*-PCL copolymers.

The representative ^{1}H NMR spectrum of PEO_{2000}-*b*-PCL_{4000}-α-TS demonstrates signals from both the PEO-*b*-PCL backbone and the α-TS moiety (Fig. 2c). The characteristic peaks of the PEO block at δ = 3.66 ppm and the PCL block at δ = 4.08 ppm are still prominent, confirming that the polymer backbone remains intact. However, additional peaks associated with the α-TS component appear. The signals at δ = 0.87–0.90 ppm correspond to the methyl groups of the α-TS, while the peaks around δ = 1.38–1.68 ppm are from both the PCL and the methylene groups of the α-TS. The succinate ester groups are represented by shifts around δ = 2.32–2.95 ppm. Similar findings were obtained with PEO_{5000}-*b*-PCL copolymers (Figure S1shows representative ^{1}H NMR spectra of plain PEO_{5000}-*b*-PCL_{10000} and α-TS-conjugated). These changes suggest the successful conjugation of α-TS to the PEO-*b*-PCL copolymer. The conjugation efficiency (%) calculated for PEO_{2000}-*b*-PCL-α-TS ranged from 99.2 to 132.5 %. For the PEO_{5000}-*b*-PCL-α-TS copolymers, however, the values ranged from 211.7 to 262.8 %.

3.3. Gel permeation chromatography (GPC)

The molecular weight distribution and dispersity of the synthesized block copolymers were assessed using GPC. The data obtained for the PEO-*b*-PCL copolymers, both before and after conjugation with α-TS, indicated successful polymer synthesis with narrow molecular weight distributions. For the PEO_{2000}-*b*-PCL and PEO_{2000}-*b*-PCL-α-TS copolymers (Table 1), the GPC results confirmed the synthesis of well-defined copolymers with polydispersity indices (PDI) ranging from 1.45 to 1.76, indicating a uniform polymer population. Similarly, PEO_{5000}-*b*-PCL and their α-TS conjugated counterparts displayed narrow molecular weight distributions (PDI = 1.41–1.75). In both groups of copolymers, there was a trend of higher PDI values for higher molecular weight copolymers (Table 1). Fig. 3 shows representative GPC chromatograms for α-TS, PEO_{5000}-*b*-PCL_{10000}, and PEO_{5000}-*b*-PCL_{10000}-α-TS. Fig. S2 shows a representative GPC chromatograms physically mixed α-TS and PEO_{5000}-*b*-PCL_{10000}-α-TS.

3.4. X-ray diffraction (XRD)

The XRD pattern of pure α-TS exhibits broad peaks indicative of a more amorphous nature, with some peaks centered around 9.6°, 15.9°, and 18.5°, corresponding to the amorphous regions of α-TS (Fig. S3a).

The XRD spectrum of PEO_{2000}-*b*-PCL_{4000} shows characteristic peaks at 2θ values around 19.3°, 21.5°, and 23.8°, which correspond to the crystalline regions of the PCL block (Fig. 4a). The peak at 21.5° showing the highest intensity relative to the others, resulting in a peak ratio of approximately 1:0.19:0.45 for 21.5°:19.3°:23.8°. Incorporating α-TS led to a minor change in the XRD pattern (Fig. 5b). The crystalline peaks of PCL are still present at similar positions (19.3°, 21.5°, and 23.8°), but their relative intensities were changed, resulting in a new peak ratio of approximately 1:0.27:0.39 for 21.3°:19.0°:23.6°. The calculated % crystallinity of PEO_{2000}-*b*-PCL_{4000} and PEO_{2000}-*b*-PCL_{4000}-α-TS were 39.49 % and 26.04 %, respectively.

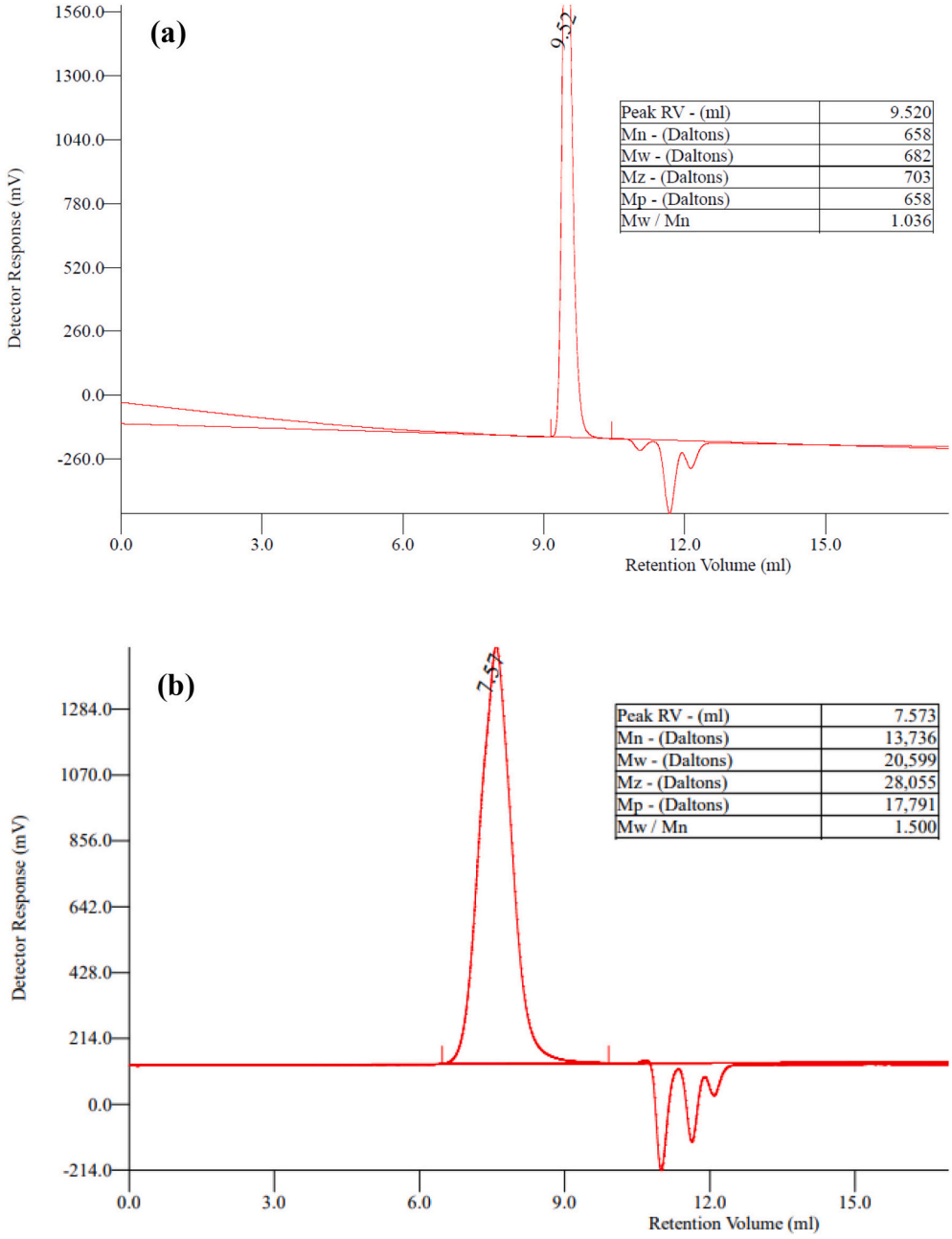

Fig. 3. Representative GPC chromatograms of α-TS (a), PEO_{5000}-b-PCL_{10000} (b) and PEO_{5000}-b-PCL_{10000}-α-TS (c).

PEO_{5000}-*b*-PCL_{10000} showed peak intensity ratios of approximately 1:0.32:0.57 for 21.5°:19.2°:23.8° (Fig. S3). The corresponding peak intensity ratios obtained with PEO_{5000}-*b*-PCL_{10000}-α-TS were 1:0.29:0.45 for 21.5°:19.3°:23.8°. The calculated % crystallinity of PEO_{5000}-*b*-PCL_{10000} and PEO_{5000}-*b*-PCL_{10000}-α-TS were 55.76 % and 56.03 %, respectively.

3.5. *Differential scanning calorimetry (DSC)*

The DSC data for α-TS shows a melting peak at 77.35 °C with an enthalpy of 87.71 J/g. This melting point reflects the crystalline nature of pure α-TS (Fig. S4a). The melting peak of the PCL crystalline phase in PEO_{2000}-*b*-PCL_{4000} was observed at 59.59 °C, with an enthalpy of 85.58 J/g, indicating a highly crystalline PCL segment (Fig. 5a). However, after the conjugation of α-TS, the melting peak shifted to 57.23 °C, and the enthalpy decreased to 84.34 J/g (Fig. 5b). The reduction in both melting temperature and enthalpy, compared to unmodified PEO_{2000}-*b*-PCL_{4000}, indicates that the incorporation of α-TS disrupts the crystalline packing of the PCL chains, leading to a decrease in the copolymer's overall crystallinity. This observation is consistent with the XRD results.

The DSC data for a representative PEO_{5000}-*b*-PCL copolymer (PEO_{5000}-*b*-PCL_{10000}) shows an endothermic peak at 61.24 °C, with a corresponding enthalpy of 84.61 J/g (Fig. S4b). This peak corresponds to the melting temperature of the PCL crystalline phase, confirming its semicrystalline nature. Similar to the trend observed with PEO_{2000}-*b*-PCL_{4000}-α-TS, the DSC data for PEO_{5000}-*b*-PCL_{10000}-α-TS shows a slightly lower melting peak at 59.99 °C and a reduced enthalpy of 75.46 J/g (Fig. S4c).

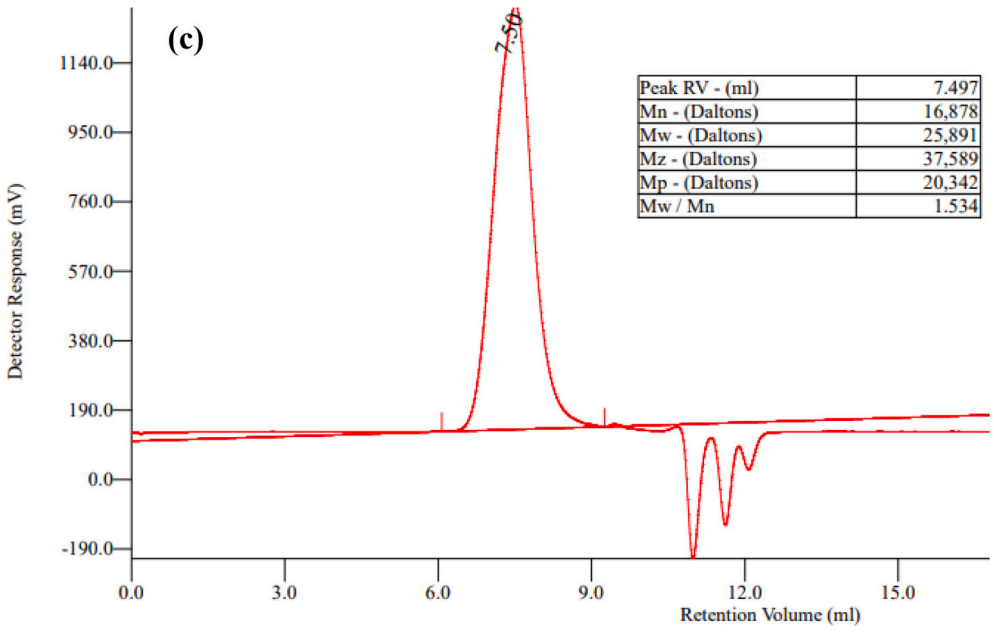

Fig. 3. (*continued*).

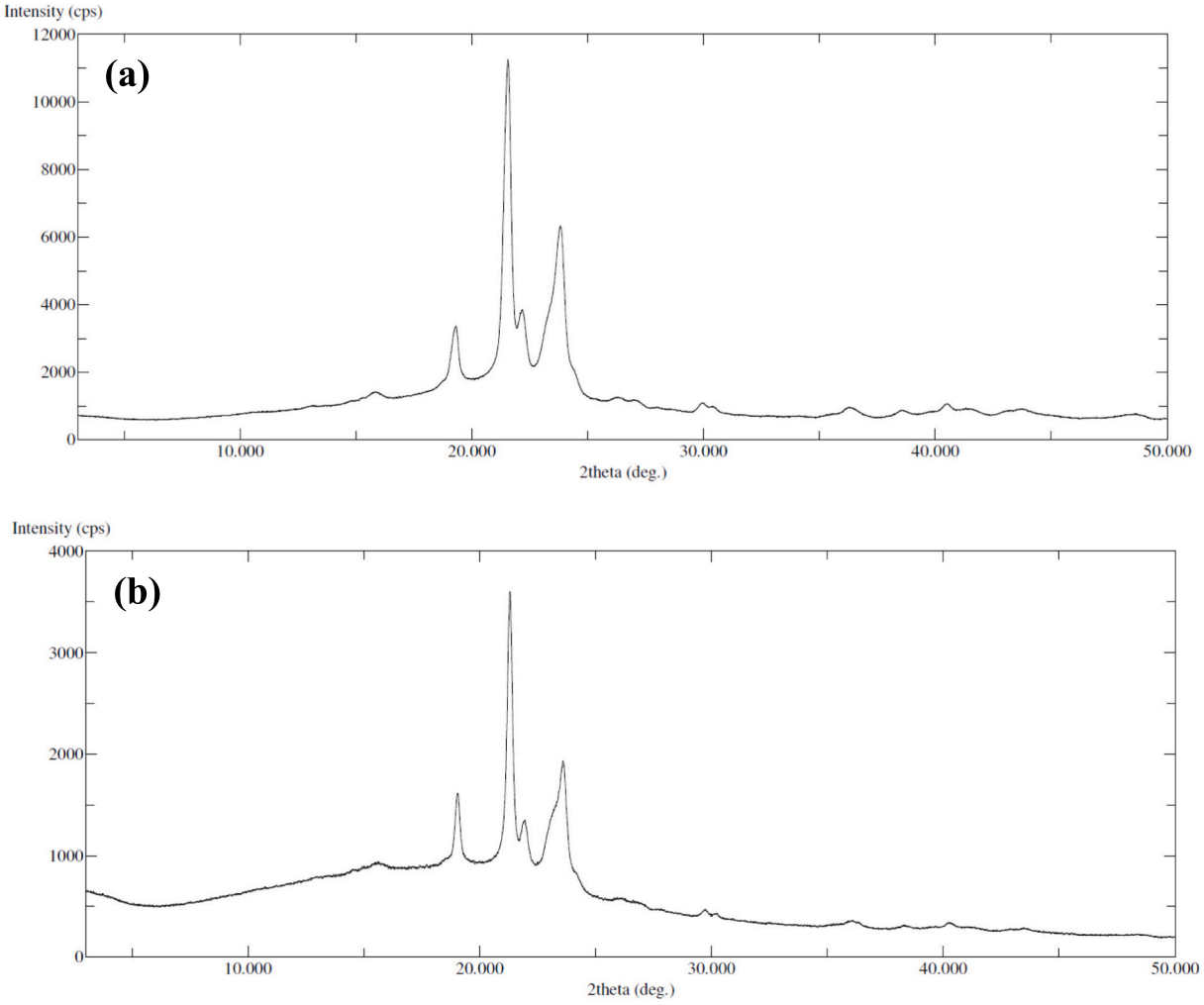

Fig. 4. Representative XRD diffractograms of PEO_{2000}-*b*-PCL_{4000} (a) and PEO_{2000}-*b*-PCL_{4000}-α-TS (b).

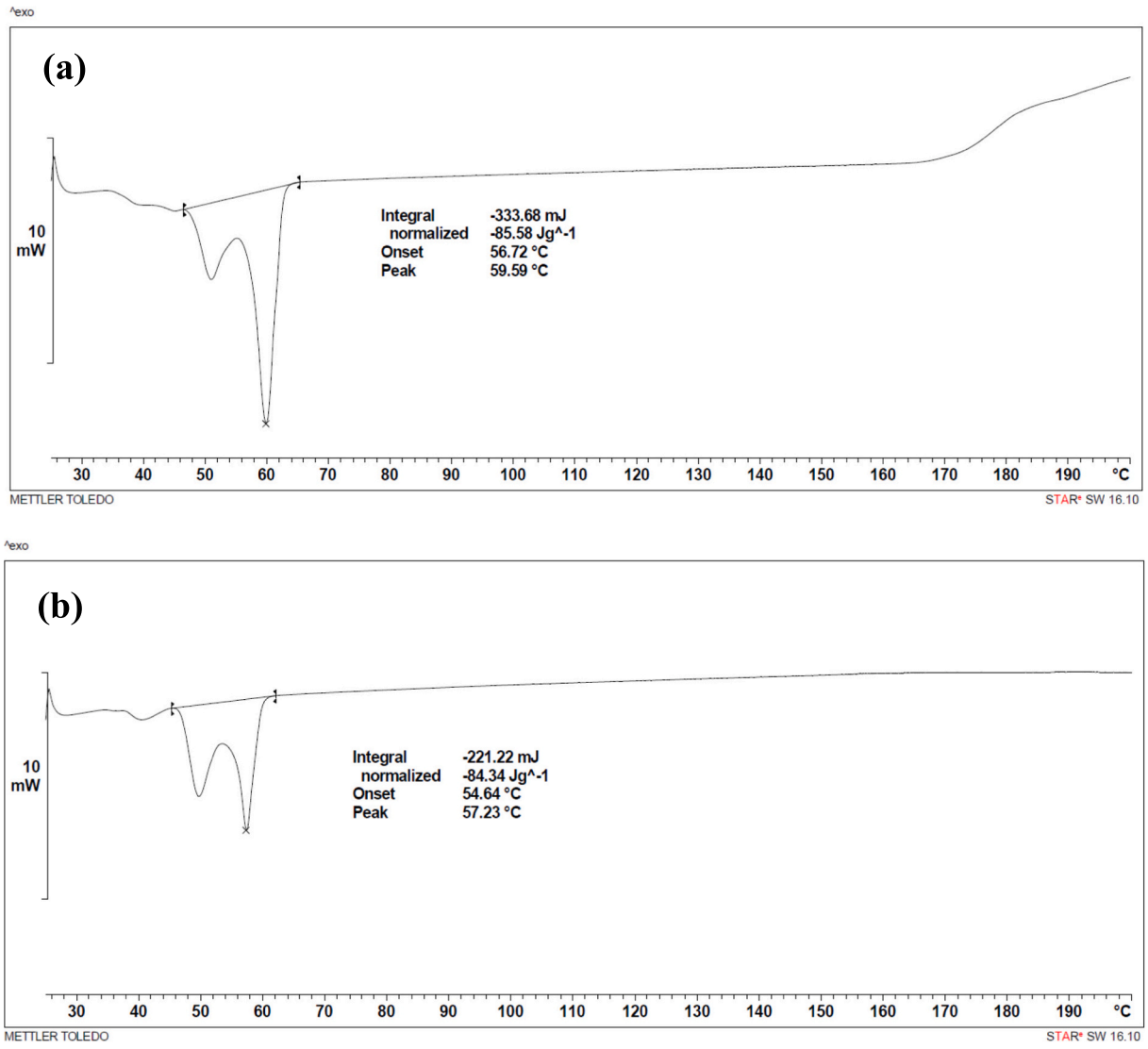

Fig. 5. Representative DSC thermograms of PEO_{2000}-*b*-PCL_{4000} (a) and PEO_{2000}-*b*-PCL_{4000}-α-TS (b).

3.6. Preparation and characterization of PEO-b-PCL-α-TS nanocarriers

The impact of polymer-drug ratios and initial drug concentrations on the encapsulation efficiency (EE%) and drug loading (DL%) for the co-polymers PEO_{2000}-*b*-PCL_{4000} and PEO_{2000}-*b*-PCL_{4000}-α-TS is summarized in Table 2. For the unmodified copolymer PEO_{2000}-b-PCL_{4000}, EE% ranged from 7.51 % to 47.72 %, depending on the polymer and drug concentrations. The highest EE% of 47.72 % was achieved with a polymer concentration of 20 mg/mL and a drug concentration of 1.5 mg/mL. The drug loading varied from 1.72 % to 3.46 % under different conditions, with the highest DL% observed at the same polymer and drug concentration combination.

For the PEO_{2000}-*b*-PCL_{4000}-α-TS copolymer, both EE% and DL% significantly improved across all conditions. The highest EE% of 90.51 % and DL% of 6.36 % were achieved at a polymer concentration of 20 mg/mL and a drug concentration of 1.5 mg/mL, indicating the positive effect of α-TS conjugation on drug encapsulation and loading. Even at lower polymer and drug concentrations, the α-TS-conjugated copolymer demonstrated superior EE% and DL% compared to its unmodified counterpart.

Table 3 presents the characteristics of rapamycin-loaded micelles formed by the PEO-*b*-PCL and PEO-*b*-PCL-α-TS copolymers, including micelle size, polydispersity index (PDI), DL%, EE%, and drug solubility. Across all formulations, the α-TS-conjugated micelles exhibited smaller sizes and lower PDI values, indicating more uniform micelle formation. For example, the micelle size for PEO_{2000}-*b*-PCL_{2000}-α-TS was 21.2 nm, significantly smaller than the 45.5 nm observed for the unmodified copolymer. Similarly, the PDI for PEO_{2000}-*b*-PCL_{2000}-α-TS was 0.281, compared to 0.662 for the unmodified micelles.

In terms of drug encapsulation and loading, α-TS-modified micelles consistently outperformed their unmodified counterparts. For instance, PEO_{2000}-*b*-PCL_{4000}-α-TS exhibited an EE% of 90.5 % and a DL% of 6.36 %, significantly higher than the EE% of 47.7 % and DL% of 3.45 % for the unmodified PEO_{2000}-*b*-PCL_{4000}. This trend was observed across all molecular weights, with α-TS-conjugated micelles showing superior DL %, EE%, and increased solubility. The solubility of rapamycin in the micelles significantly increased upon α-TS conjugation, with PEO_{2000}-*b*-PCL_{4000}-α-TS achieving a drug solubility of 1357.5 μg/mL, compared to 715.5 μg/mL for the unmodified counterpart.

Rapamycin-loaded PEO_{5000}-*b*-PCL_{10000}-α-TS came next in terms of EE% and DL%, achieving 58.0 % and 4.17 %, respectively. These values are approximately 78 % and 74 % higher than those obtained with PEO_{5000}-*b*-PCL_{10000} micelles, respectively (Table 3). Interestingly, the highest EE% and DL% were obtained with micelles prepared from co-polymers having a PEO:PCL ratio of 1:2.

The morphology of both the unloaded and rapamycin-loaded

Table 2
Impact of polymer-drug ratios and initial concentrations on drug encapsulation efficiency (EE%) and drug loading (DL%).

Copolymer	Polymer concentration (mg/mL)	Drug concentration (mg/mL)	DL (%)	EE (%)
PEO_{2000}-*b*-PCL_{4000}	5	1.3	2.25 ± 0.13	8.68 ± 0.50
	10	3.0	2.20 ± 0.08	7.51 ± 0.28
	15	1.5	2.09 ± 0.03	21.35 ± 0.33
	20	2.0	1.72 ± 0.15	17.51 ± 1.55
PEO_{2000}-*b*-PCL_{4000}–α-TS	20	1.5	3.46 ± 0.67	47.72 ± 9.02
	5	1.3	3.04 ± 0.67	12.08 ± 2.61
	10	3.0	3.37 ± 0.49*	11.63 ± 1.65*
	15	1.5	3.94 ± 0.59*	41.05 ± 5.89*
	20	2.0	3.92 ± 0.17*	40.76 ± 1.74*
	20	1.5	6.36 ± 0.40*	90.51 ± 5.38*

The polymer and drug concentrations are per mL deionized water with a fixed organic:aqueous ratio of 1:6. * The differences between PEO_{2000}-*b*-PCL_{4000} and their PEO_{2000}-*b*-PCL_{4000}–α-TS counterparts were statistically significant ($p < 0.05$; Student's *t*-test).

micelles was examined using TEM, which confirmed their spherical shape (Fig. 6). The measured diameters of the micelles were consistent with the results obtained from DLS analysis.

3.7. *In vitro drug release from PEO-b-PCL-α-TS nanocarriers*

The *in vitro* release profile of rapamycin from selected rapamycin-loaded micelles was investigated. Among the prepared formulations, PEO_{2000}-*b*-PCL_{4000} and PEO_{2000}-*b*-PCL_{4000}-α-TS micelles, which demonstrated the highest EE%, were chosen for the study.

Fig. 7 presents the results, comparing the rapamycin release from an ethanolic solution to that from micellar formulations. The ethanolic solution exhibited a burst release of 65 % within the first 5 h that peaked at 12 h reaching nearly 78 %, followed by a decline in rapamycin concentration over the testing period to reach approximately 40 %. The mean concentration of the drug inside the dialysis bag at the end of the 72-h study was approximately 1.6 μg/mL, representing only 0.32 % of the initial drug concentration (500 μg/mL). This finding strongly indicates that significant drug degradation occurred. Notably, the mean back-calculated percentage of drug content (accounting for both the media and the contents inside the bag) was 78 %, confirming that 22 % of the drug was degraded.

In contrast, the PEO_{2000}-*b*-PCL_{4000} and PEO_{2000}-*b*-PCL_{4000}-α-TS micelles demonstrated a sustained release of rapamycin. During the initial 5 h, rapamycin release was 14 % and 21 % from PEO_{2000}-*b*-PCL_{4000} and PEO_{2000}-*b*-PCL_{4000}-α-TS micelles, respectively. At 12 h, the mean % drug release reached around 21 % and 34 % from PEO_{2000}-*b*-PCL_{4000} and PEO_{2000}-*b*-PCL_{4000}-α-TS micelles, respectively. At 72 h, the PEO_{2000}-*b*-PCL_{4000} micelles released 41 % of the drug, which was relatively lower than the % release observed with PEO_{2000}-*b*-PCL_{4000}-α-TS micelles (50 %). The difference was statistically significant ($p < 0.05$; Student's *t*-test). The drug concentrations remaining inside the dialysis bag for PEO_{2000}-*b*-PCL_{4000} and PEO_{2000}-*b*-PCL_{4000}-α-TS micelles were 326.7 and 211.8 μg/mL, respectively, corresponding to approximately 65.3 % and 42.4 % of the initial drug concentration. These findings strongly indicate that the drug remained intact throughout the study when encapsulated in the micellar formulation.

To better simulate physiological conditions, the release behavior of

Table 3
Characteristics of the developed rapamycin-loaded PEO-*b*-PCL and PEO-*b*-PCL-α-TS micelles.

Copolymer	Micelle size (nm)	PDI	DL (%)	EE (%)	Drug solubility (μg/mL)
PEO_{2000}-*b*-PCL_{2000}	45.5 ± 1.4[b]	0.662 ± 0.049	1.86 ± 0.31[b]	25.3 ± 4.1 [b]	379.5 ± 61.5[b]
PEO_{2000}-*b*-PCL_{2000}–α-TS	21.2 ± 2.1*[a,b,c]	0.281 ± 0.051*[a]	2.79 ± 0.22*[a,b]	38.3 ± 3.0* [a,b]	574.5 ± 45.0* [a,b]
PEO_{2000}-*b*-PCL_{4000}	33.2 ± 2.4[a,c]	0.254 ± 0.063[a]	3.45 ± 0.67[a,c]	47.7 ± 9.0 [a,c]	715.5 ± 135.0 [a,c]
PEO_{2000}-*b*-PCL_{4000}–α-TS	18.9 ± 2.2*[a]	0.237 ± 0.056[a]	6.36 ± 0.40*[a,b,c]	90.5 ± 5.4*[a,b,c]	1357.5 ± 81.0* [a,b,c]
PEO_{2000}-*b*-PCL_{6000}	41.9 ± 3.7[b]	0.237 ± 0.098[a]	2.40 ± 0.07[b]	32.8 ± 0.9[b]	491.7 ± 13.1[b]
PEO_{2000}-*b*-PCL_{6000}–α-TS	27.3 ± 2.7*[a]	0.285 ± 0.065[a]	4.12 ± 0.27*[a]	57.3 ± 3.7*[a]	860.1 ± 54.9*[a]
PEO_{5000}-*b*-PCL_{5000}	69.1 ± 3.3[e,f]	0.270 ± 0.035[d]	1.67 ± 0.03	22.7 ± 0.4[e]	340.5 ± 6.0
PEO_{5000}-*b*-PCL_{5000}–α-TS	62.7 ± 5.1	0.379 ± 0.061	2.46 ± 0.19*	33.6 ± 2.5*[d]	504.0 ± 37.5*[d]
PEO_{5000}-*b*-PCL_{10000}	110.8 ± 2.0[d]	0.412 ± 0.011[c]	2.39 ± 0.22	32.6 ± 3.0[d,f]	489.0 ± 45.0[d,f]
PEO_{5000}-*b*-PCL_{10000}–α-TS	106.3 ± 2.2*[d]	0.379 ± 0.043[c]	4.17 ± 0.86*	58.0 ± 11.5*[d,e,f]	870.0 ± 172.5* [d,e,f]
PEO_{5000}-*b*-PCL_{15000}	116.9 ± 10.4[d]	0.355 ± 0.043	1.42 ± 0.29	19.2 ± 3.8	287.3 ± 57.2
PEO_{5000}-*b*-PCL_{15000}–α-TS	102.2 ± 1.1*[d]	0.281 ± 0.051[e]	1.74 ± 0.13	23.6 ± 1.7	353.4 ± 25.3

The statistical analysis was performed using one-way ANOVA followed by Tukey's multiple comparisons test. [a] Differences were considered significant at $p < 0.05$ compared to PEO_{2000}-*b*-PCL_{2000}. [b] Differences were considered significant at $p < 0.05$ compared to PEO_{2000}-*b*-PCL_{4000}. [c] Differences were considered significant at $p < 0.05$ compared to PEO_{2000}-*b*-PCL_{6000}. [d] Differences were considered significant at $p < 0.05$ compared to PEO_{5000}-*b*-PCL_{5000}. [e] Differences were considered significant at $p < 0.05$ compared to PEO_{5000}-*b*-PCL_{10000}. [f] Differences were considered significant at $p < 0.05$ compared to PEO_{5000}-*b*-PCL_{15000}.

rapamycin from micelles was further evaluated in the presence of bovine serum albumin (BSA, 40 mg/mL) at 37 °C. Fig. 7b displays the % cumulative release profiles of rapamycin from PEO_{2000}-*b*-PCL_{4000} micelles, PEO_{2000}-*b*-PCL_{4000}-α-TS micelles, and a rapamycin solution. As anticipated, the rapamycin solution exhibited a rapid release, achieving over 90 % drug release within the first 2 h. This rapid release confirms that sink conditions were maintained, and that drug diffusion was not hindered by the dialysis membrane.

In contrast, the PEO_{2000}-*b*-PCL_{4000} and PEO_{2000}-*b*-PCL_{4000}-α-TS micelles demonstrated a sustained release profile for rapamycin. Within the first 4 h, 53.22 % and 68.97 % of the drug was released from PEO_{2000}-*b*-PCL_{4000} and PEO_{2000}-*b*-PCL_{4000}-α-TS micelles, respectively. By 12 h, the cumulative drug release increased to 70.91 % for PEO_{2000}-*b*-PCL_{4000} and 87.44 % for the α-TS modified counterpart. Nearly 100 % drug release from both micellar formulations was achieved within 48 h.

3.8. *In vitro micelle stability and drug leakage studies*

The stability of rapamycin-loaded PEO-*b*-PCL and PEO-*b*-PCL-α-TS micelles was evaluated under two temperature conditions, RT and 4 ± 1 °C over a six-month period. Fig. 8a and b illustrate the changes in micelle size during storage at 4 °C and RT, respectively.

As shown in Fig. 8, the average size of rapamycin-loaded PEO_{2000}-*b*-PCL_{4000} micelles significantly increased after one month of storage at RT and after six months at 4 °C. However, the PDI remained relatively stable

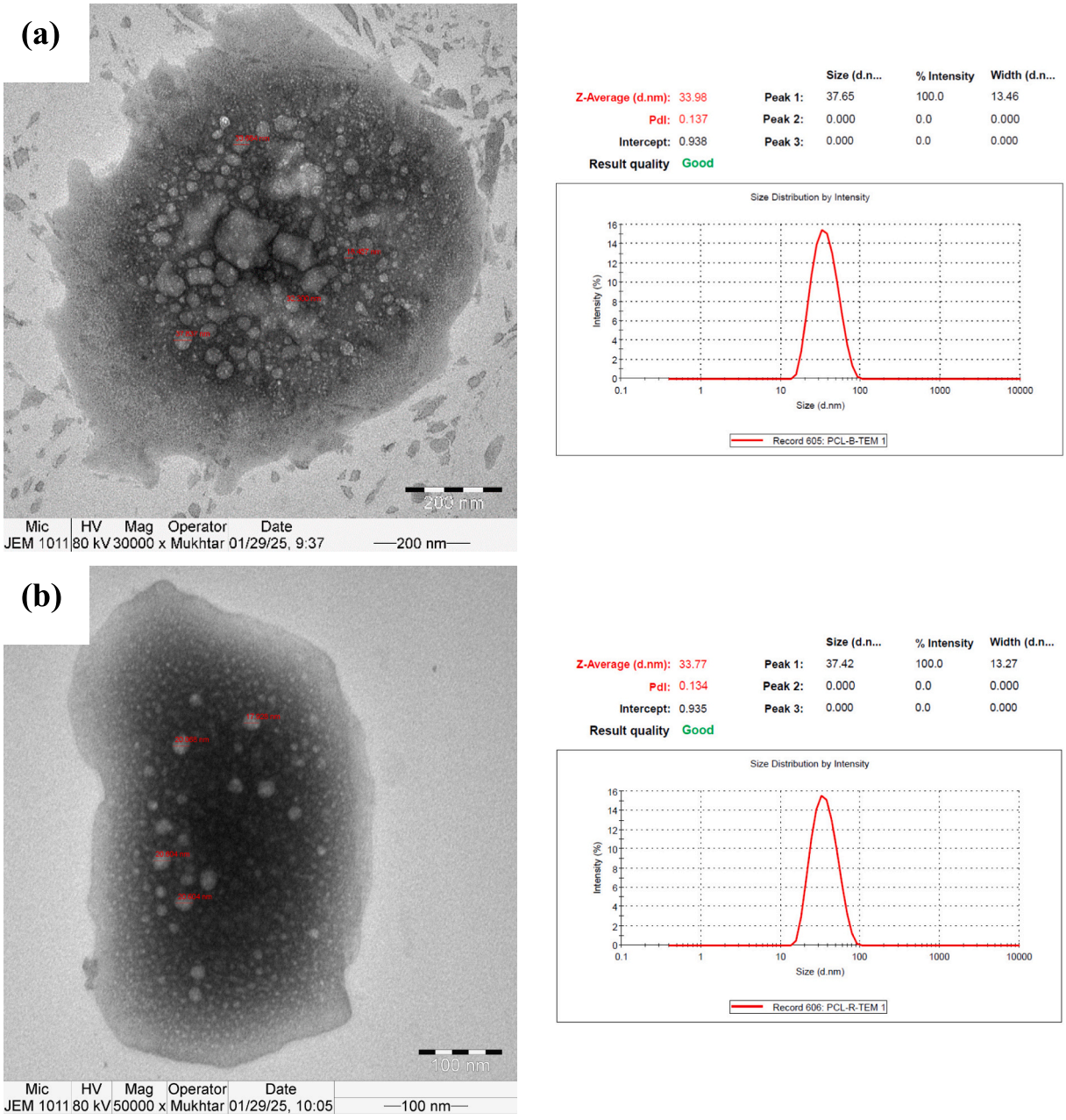

Fig. 6. TEM images of unloaded PEO_{2000}-*b*-PCL_{4000} (a), rapamycin-loaded PEO_{2000}-*b*-PCL_{4000} (b), unloaded PEO_{2000}-*b*-PCL_{4000}-α-TS (c), and rapamycin-loaded PEO_{2000}-*b*-PCL_{4000}-α-TS (d). The corresponding DLS data for each sample is displayed adjacent to its respective TEM image, providing particle size distribution and polydispersity index.

throughout the 6-month storage period, regardless of temperature. In contrast, rapamycin-loaded PEO-*b*-PCL-α-TS micelles exhibited a significant increase in both size and PDI within two weeks at both storage conditions.

Regarding drug retention, Fig. 9 indicates that rapamycin-loaded micelles were more stable at 4 °C than at RT. The percentage of rapamycin retained in PEO_{2000}-*b*-PCL_{4000} micelles dropped below 90 % within the first week of storage at RT. In contrast, at 4 °C, drug content remained above 90 % for one month before decreasing to 84.5 % two months later. Rapamycin-loaded PEO-b-PCL-α-TS micelles displayed a similar stability profile to the α-TS-free formulation at RT but exhibited greater stability at 4 °C, retaining over 90 % of rapamycin for up to 3 months. Drug content then dropped slightly below 90 % after 6 months of storage.

3.9. *In vitro cytotoxicity study*

The MTT assay results presented in Fig. 10 demonstrate the cytotoxic effects of rapamycin-loaded PEO_{2000}-*b*-PCL_{4000}-α-TS and PEO_{2000}-*b*-PCL_{4000} micelles, as well as their unloaded counterparts, on human fibroblast cells (HFF1) and two human cancer cell lines (A549 and HCT116) after 24 and 72 h of treatment.

The results show that the unloaded PEO_{2000}-*b*-PCL_{4000}-α-TS and PEO_{2000}-*b*-PCL_{4000} micelles did not induce any noticeable toxicity against HFF1 cells after 24 h incubation, with % viability in the range of ~80–106 % (Fig. 10). After 72 h incubation, the % viability obtained with the unloaded PEO_{2000}-*b*-PCL_{4000} micelles was ≥70 % up to concentrations equivalent to 25 μM. However, at higher concentrations (50 and 100 μM), the % viability dropped slightly to ~62 %. Unloaded

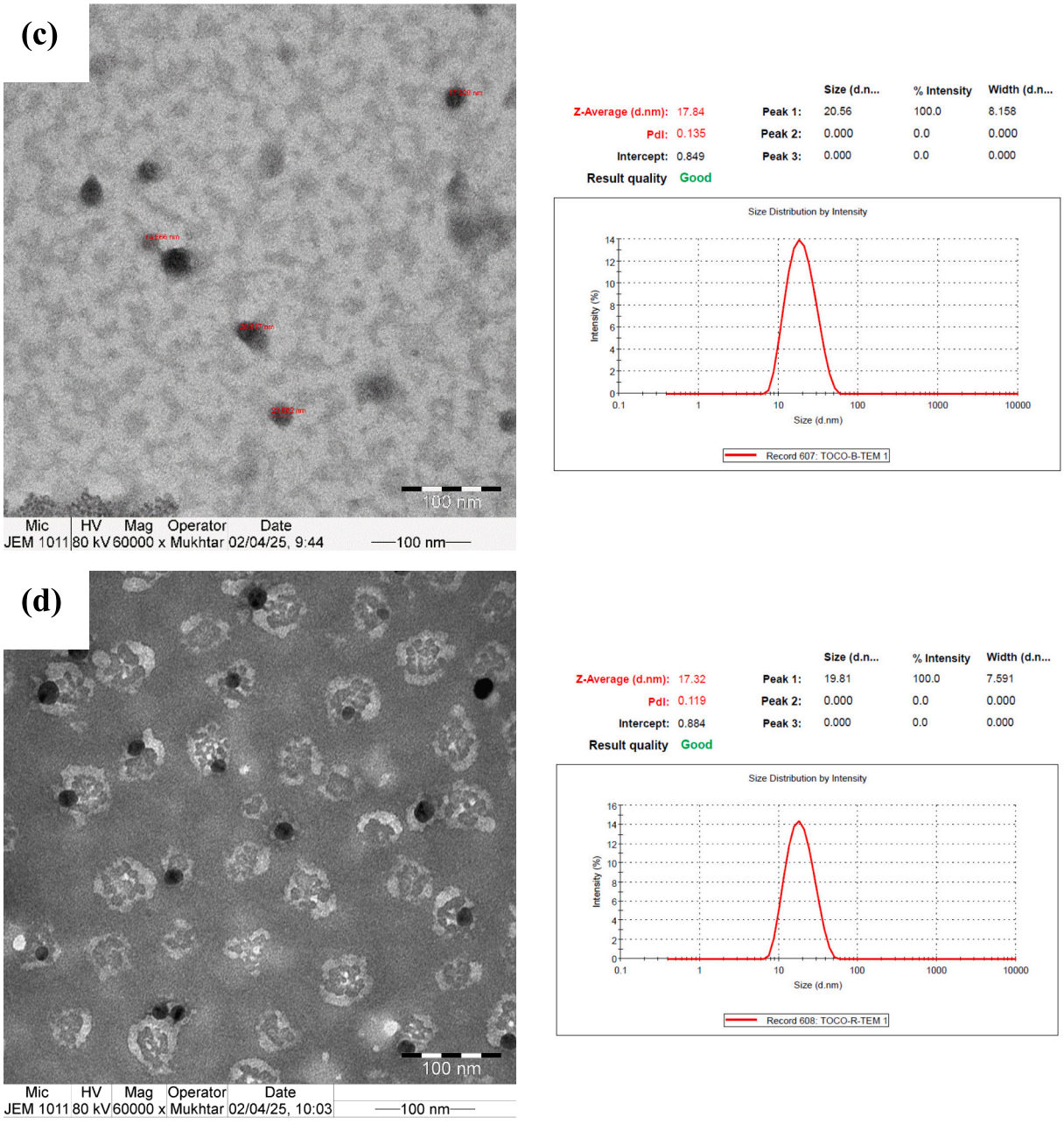

Fig. 6. (*continued*).

PEO_{2000}-*b*-PCL_{4000}-α-TS tended to have higher % viability (≥ 90 %) up to 25 μM, which dropped to reach ~75 % and ~ 62 % at 50 and 100 μM, respectively (Fig. 10). The drug-loaded micelles followed the same trend as their unloaded counterparts. Specifically, the %viability obtained with rapamycin-loaded PEO_{2000}-*b*-PCL_{4000}-α-TS ranged from 70 to 85 % except for the highest concentration (100 μM), where it dropped to ~62 %. The range of % viability observed with rapamycin-loaded PEO_{2000}-*b*-PCL_{4000} micelles was 55–69 %, which dropped at the highest concentration to reach ~48 % (Fig. 10).

In A549 cells, rapamycin-loaded micelles demonstrated a time-dependent cytotoxicity (Fig. 10). The mean IC_{50} values calculated for rapamycin-loaded PEO_{2000}-*b*-PCL_{4000} micelles following 24 and 72 h incubation were 27.77 and 9.18 μM, respectively. The corresponding values for rapamycin-loaded PEO_{2000}-*b*-PCL_{4000}-α-TS were relatively higher, 71.85 and 29.51 μM, respectively (Table 4). Interestingly, the unloaded micelles also showed cytotoxic effects but with IC_{50} values relatively higher than those obtained with the drug-loaded counterparts (Table 4).

In HCT116 cells, rapamycin-loaded micelles demonstrated a time-dependent cytotoxicity (Fig. 10). The mean IC_{50} values calculated for rapamycin-loaded PEO_{2000}-*b*-PCL_{4000} micelles following 24 and 72 h incubation were 63.58 and 27.19 μM, respectively. The corresponding values for rapamycin-loaded PEO_{2000}-*b*-PCL_{4000}-α-TS were relatively lower, 52.61 and 24.29 μM, respectively (Table 4). Similar to the findings in A549 cells, the unloaded micelles also showed cytotoxic effects on HCT116 cells. However, based on the calculated IC_{50} values, the effects were lower than those obtained with rapamycin-loaded micelles (Table 4).

4. Discussion

PEO-*b*-PCL is a member of the PEO-*b*-poly(ester) block copolymer family. Compared to other core-forming blocks in this category –such as poly(lactic-*co*-glycolic acid) (PLGA), poly(lactic acid) (PLA) and poly

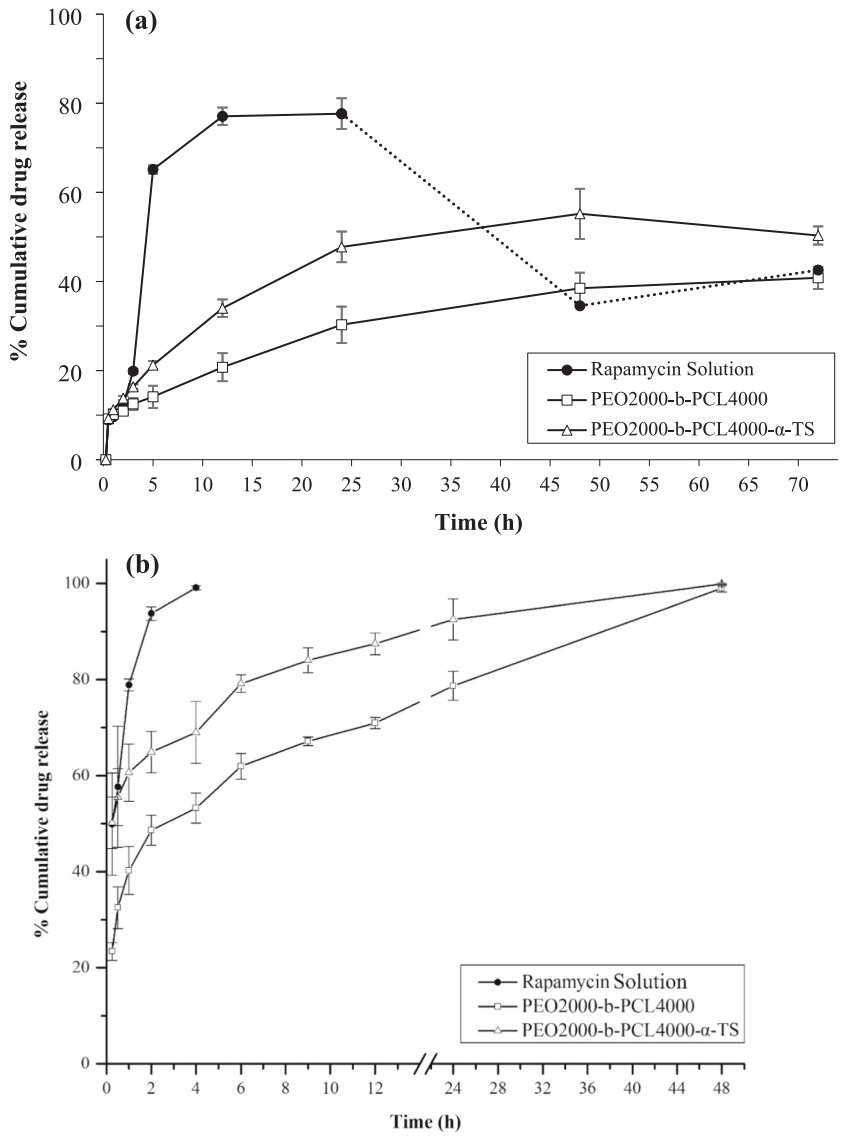

Fig. 7. (a) *In vitro* release profile of rapamycin in hydrotropic medium (without BSA) from the ethanolic solution, PEO_{2000}-*b*-PCL_{4000} micelles, and PEO_{2000}-*b*-PCL_{4000}-α-TS micelles. (b) *In vitro* release profile of rapamycin in the presence of BSA (40 mg/mL) from the drug solution, PEO_{2000}-*b*-PCL_{4000} micelles, and PEO_{2000}-*b*-PCL_{4000}-α-TS micelles.

(lactic-*co*-caprolactone) (PLCL)– PCL offers favorable characteristics for sustained drug delivery (Woodruff and Hutmacher, 2010). It has a relatively low glass transition temperature and a slow degradation rate, both of which contribute to prolonged stability and extended drug release profiles (Woodruff and Hutmacher, 2010). Additionally, PCL exhibits excellent compatibility with a broad range of hydrophobic drugs, including rapamycin (Aliabadi and Lavasanifar, 2006; Forrest et al., 2006). The semi-crystalline nature of PCL further distinguishes it from amorphous polyesters like PLGA by providing kinetic stabilization of the micellar core, thereby facilitating sustained drug release from PCL-based nanocarriers (Theerasilp and Nasongkla, 2013; Woodruff and Hutmacher, 2010).

The degradation of PLGA and PLA results in the accumulation of lactic and glycolic acid, which can significantly lower the local pH and trigger autocatalytic degradation, a self-accelerating process in which the acidic byproducts further catalyze polymer breakdown (Zweers et al., 2004). This phenomenon can lead to premature drug release and destabilization of the micellar structure. In contrast, PCL exhibits a more neutral and gradual degradation profile, avoiding local acidification and thereby better preserving the structural integrity of both the carrier and the encapsulated drug. These attributes render PCL a more suitable candidate for the development of long-circulating, physically stable PEO-*b*-poly(ester) micellar nanocarriers (Geng and Discher, 2005; Woodruff and Hutmacher, 2010).

The results obtained from the various analytical techniques demonstrate the successful synthesis of PEO-*b*-PCL copolymers and their conjugation to α-tocopheryl succinate. ^{1}H NMR (Figs. 2 and S1) provided direct evidence of the conjugation reaction, with characteristic peaks from both α-TS and the polymer backbone observed in the final product. The GPC data further validated the conjugation by showing an increase in molecular weight and a slight broadening of the PDI, both expected due to the addition of the bulky α-TS moiety (Figs. 3 and S2). The calculated % conjugation efficiency of α-TS to PEO_{2000}-*b*-PCL copolymers were close to 100 %. However, the larger molecular weight copolymers, *i.e.*, PEO_{5000}-*b*-PCL, showed higher values (~ 212–263 %). This could be attributed to the inefficient extraction of the unreacted α-TS from these high molecular weight copolymers using the conventional liquid-liquid extraction applied in this study even after more than two rounds of purifications were performed. More efficient extraction methods are needed for those copolymers, *e.g.*, Soxhlet extraction.

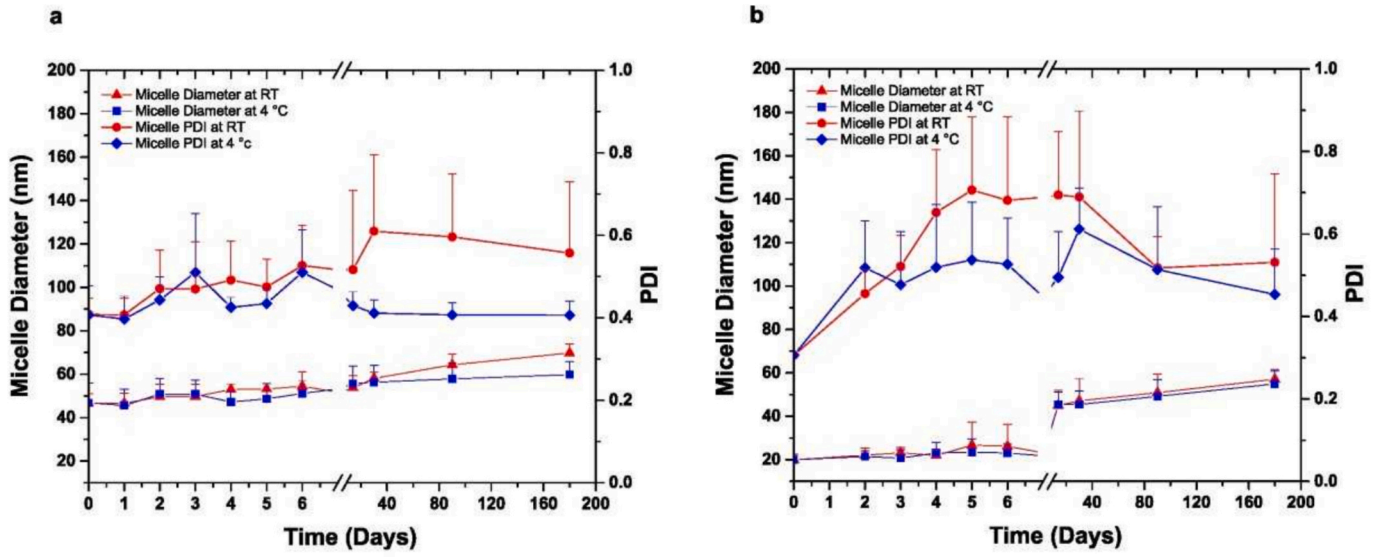

Fig. 8. Changes of size and polydispersity index (PDI) of rapamycin-loaded PEO_{2000}-*b*-PCL_{4000} (a) and rapamycin-loaded PEO_{2000}-*b*-PCL_{4000}-α-TS (b) upon storage at 4 °C and room temperature (RT). Each data point represents the mean ± SD ($n = 3$).

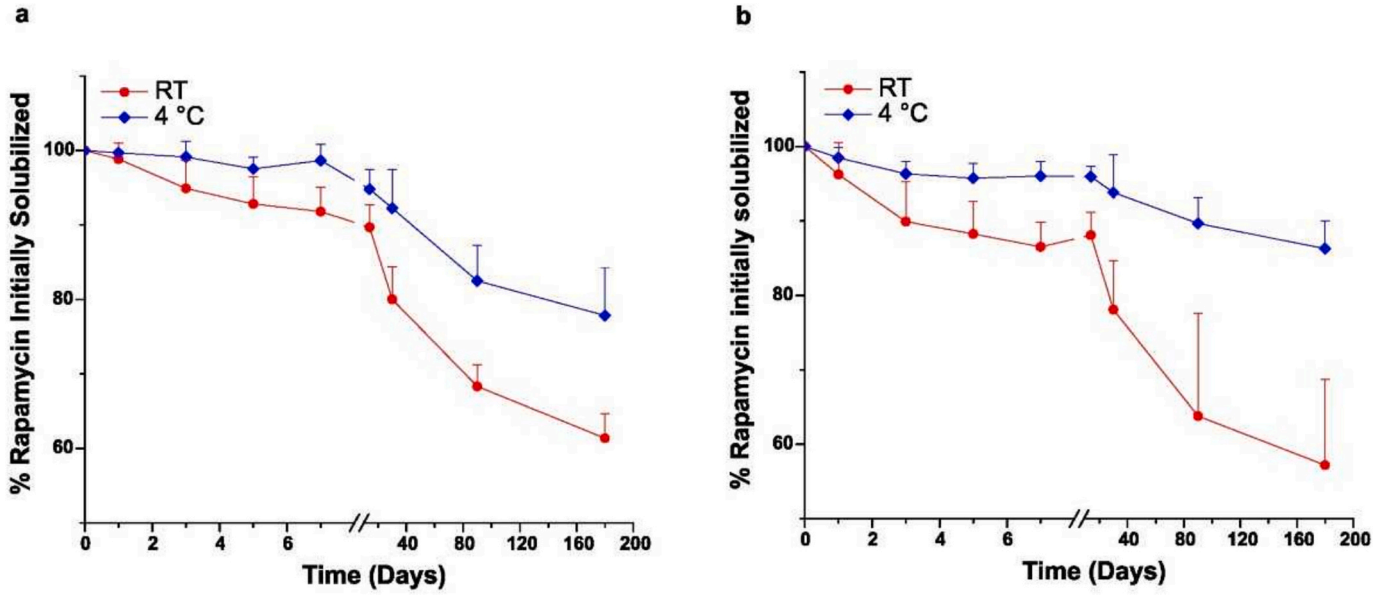

Fig. 9. % Drug remaining in rapamycin-loaded PEO_{2000}-*b*-PCL_{4000} micelles (a) and rapamycin-loaded PEO_{2000}-*b*-PCL_{4000}-α-TS micelles (b) upon storage at 4 °C and room temperature (RT). Each data point represents the mean ± SD (n = 3).

The structural information from XRD (Figs. 4 and S3) and the thermal analysis results obtained from DSC (Figs. 5 and S4) are in good agreement, showing that the conjugation of α-TS leads to a reduction in the crystallinity of the PCL block. This was evident from the decrease in the melting temperature and enthalpy values in the DSC thermograms, as well as the reduction in intensity of the PCL crystalline peaks in the XRD patterns.

PEO-*b*-PCL-α-TS micelles showed significantly higher drug solubility compared to their non-modified counterparts (Table 3). Specifically, the solubility of rapamycin in PEO_{2000}-*b*-PCL_{4000}-α-TS micelles was 1357.5 μg/mL, nearly double that of the unmodified micelles. This improved solubility likely results from the reduced crystallinity of the PCL block upon α-TS conjugation, as suggested by the DSC and XRD findings, which promote the formation of a more amorphous structure that can accommodate higher drug loads. Another important factor is the presence of alpha-tocopherol moiety in the core of the micelles, which has been shown to be compatible with rapamycin and increases its loading into PEO-*b*-PCL-based micelles (Forrest et al., 2006; Yanez et al., 2008). Specifically, in the work reported by Forrest et al. (2006) (Forrest et al., 2006) on rapamycin-loaded PEO_{5000}-*b*-PCL_{10000} micelles with physically added α-tocopherol, the highest EE% and DL% were 73 % and 10.0 %, respectively. In our current study, the corresponding values obtained with PEO_{5000}-*b*-PCL_{10000}-α-TS were 58.0 % and 4.17 %, respectively. Nonetheless, it should be noted that in the work of Forrest et al., the molecule was α-tocopherol (without succinate) and that it was physically loaded (not chemically conjugated). Specifically, α-tocopherol was physically added to the PEO-*b*-PCL copolymers in a 20:1 M ratio of α-tocopherol to polymer (Forrest et al., 2006). This means that 20 molecules of α-tocopherol (molecular weight ≈ 430 Da) were added for every one molecule of PEO_{5000}-*b*-PCL_{10000} (molecular weight ≈ 15,000 Da), which translates to 36.44 % α-tocopherol in this system. In our study, however, the calculated conjugation efficiency of α-TS (molecular

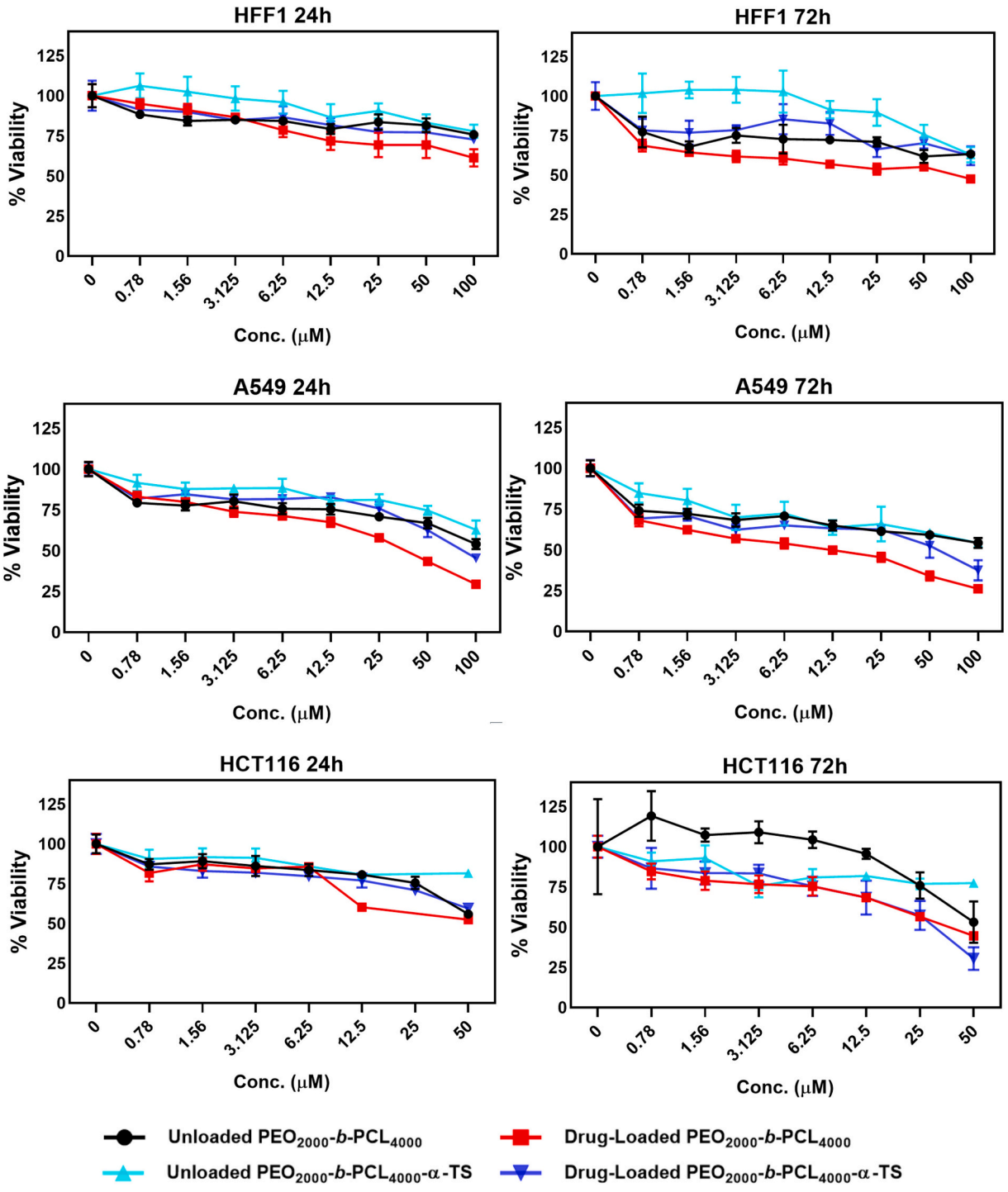

Fig. 10. % Viability of human fibroblast cells (HFF1), human lung carcinoma epithelial cells (A549), and human colon adenocarcinoma cells (HCT116) determined by MTT assay after 24 h (left panel) and 72 h (right panel) of incubation with rapamycin-loaded PEO_{2000}-*b*-PCL_{4000} and rapamycin-loaded PEO_{2000}-*b*-PCL_{4000}-α-TS. A molar equivalent unloaded micelles were also used. Each data point represents the mean ± SD (n = 3).

weight ≈ 530 Da) in PEO_{5000}-*b*-PCL_{10000}-α-TS was approximately 248 %, resulting in a ratio of ~1:2.5 between the PCL chain and the α-tocopheryl moiety. Therefore, for PEO_{5000}-*b*-PCL_{10000}-α-TS copolymers, only 8.53 % of the total mass of the system corresponds to the α-TS moiety.

In vitro dissolution or release testing of poorly water-soluble drug formulations poses significant challenges due to inadequate drug solubility in the media, preventing the achievement of sink conditions required for effective testing. One strategy to tackle these challenges is to enhance the aqueous solubility of the drug in the receiving phase using facilitated hydrotropy (Yalkowsky, 1999).

Previous studies have shown that N,N-diethylnicotinamide (DENA) was an effective hydrotropic agent for accelerated release of paclitaxel, another poorly water-soluble drug (Baek et al., 2004; Lee et al., 2003). Furthermore, Othman et al. investigated the *in vitro* release profile of rapamycin-loaded PCL nanoparticles, utilizing DENA as a hydrotropic agent (Othman et al., 2016). The solubilizing effect of DENA was further enhanced by the addition of ethanol and Tween 20 (polysorbate 20) to the dissolution medium. In the present study, a similar dissolution medium was employed to evaluate the *in vitro* release profile of rapamycin-loaded micelles.

Table 4
The mean IC_{50} (μM) values of the developed rapamycin-loaded PEO-*b*-PCL and PEO-*b*-PCL-α-TS micelles, as well as the molar equivalent unloaded micelles, after incubation for 24 and 72 h with A549 and HCT116 cancer cell lines.

Type of Cells (Incubation Time)	IC_{50} (μM)			
	Unloaded PEO_{2000}-*b*-PCL_{4000}	Drug-Loaded PEO_{2000}-*b*-PCL_{4000}	Unloaded PEO_{2000}-*b*-PCL_{4000}-α-TS	Drug-Loaded PEO_{2000}-*b*-PCL_{4000}-α-TS
HFF1 (24 h)	>100	90.07	>100	>100
HFF1 (72 h)	>100	24.43	>100	>100
A549 (24 h)	74.83	27.77	131.80	71.85
A549 (72 h)	46.59	9.18	53.03	29.51
HCT116 (24 h)	58.68	63.58	206.70	52.61
HCT116 (72 h)	84.17	27.19	95.90	24.29

The results demonstrated that both PEO_{2000}-*b*-PCL_{4000} and PEO_{2000}-*b*-PCL_{4000}-α-TS significantly slowed down the release of encapsulated rapamycin compared to its ethanolic solution (Fig. 7a). However, as shown in Fig. 7a, α-TS conjugation led to a faster release of rapamycin compared to the unmodified PEO-*b*-PCL micelles. This observation is attributed to the structural changes induced by α-TS conjugation. Specifically, as demonstrated by XRD and DSC analyses, α-TS conjugation reduced the crystallinity of the PCL core, leading to a less ordered and more amorphous core environment. This structural disruption likely enhances the diffusion rate of the encapsulated drug, thereby accelerating its release.

Rapamycin is known to be susceptible to chemical degradation especially in aqueous environments (Merciadez et al., 2011; Oyler et al., 2012; van der Wagt et al., 2024). For instance, in a recent study by van der Wagt et al. (2024) (van der Wagt et al., 2024), the chemical stability of rapamycin was evaluated in PBS (pH 7.4) at varying temperatures (4 °C, 22 °C and 37 °C). The drug remained stable for at least 168 h at 4 °C (van der Wagt et al., 2024). However, its stability was temperature-dependent, with significant reduction in the amount of the remaining drug at 22 °C and 37 °C, as indicated by the estimated degradation half-lives of 58.9 ± 1.3 h (22 °C) and 5.7 ± 0.4 h. Additionally, rapamycin rapidly degraded in serum at 37 °C with an estimated degradation half-life of 5.8 ± 0.7 h. Interestingly, the drug was stable in whole blood for the entire 168-h incubation period. This was attributed to its sequestration within red blood cells, which prevented it from hydrolytic degradation (van der Wagt et al., 2024). In fact, rapamycin has been shown to exhibit a very high affinity for red blood cells, with approximately 95 % of the drug in whole blood distributed within those cells (Trepanier et al., 1998).

Our *in vitro* release study demonstrated that rapamycin-loaded micelles offered significantly improved stability compared to an ethanolic solution, which degraded rapidly, losing 22 % of its content within 72 h. Encapsulation within micelles effectively minimized the exposure of the drug to the aqueous environment, thereby providing a protective mechanism against hydrolytic degradation, similar to its sequestration in red blood cells observed in van der Wagt et al. (2024) study (van der Wagt et al., 2024).

When comparing the drug release profiles in the presence (Fig. 7b) and absence (Fig. 7a) of BSA, both micellar formulations exhibited comparable release trends. In both media, PEO_{2000}-*b*-PCL_{4000}-α-TS micelles exhibited a higher percentage of rapamycin release compared to unmodified PEO_{2000}-*b*-PCL_{4000} micelles at nearly all time points.

Although the absolute % release values were consistently higher in the BSA-containing medium, this difference is likely due to enhanced drug solubilization and protein interactions, rather than a fundamental shift in release mechanism. The similarity in relative release trends across both conditions indicates that the micellar architecture remains the dominant factor controlling release kinetics, which are primarily governed by diffusion.

In the presence of BSA, the drug release process is governed by two concurrent mass equilibria: (1) the equilibrium between rapamycin encapsulated within the micelles and the free drug in the aqueous phase, and (2) the equilibrium between the free drug and albumin-bound rapamycin. BSA, present at physiological concentration, acts as a drug-accepting sink by dynamically binding the released rapamycin, thereby lowering the free drug concentration inside the dialysis bag. This reduction maintains a concentration gradient that favors further diffusion of rapamycin from the micelles. Importantly, only the unbound (free) drug is capable of diffusing across the dialysis membrane, while BSA and micelles remain confined within the bag. Consequently, the repeated replacement of the external medium continuously removes the free drug, which in turn shifts the equilibrium toward the dissociation of albumin-bound rapamycin and further drug release from the micelles. This mechanism explains the enhanced cumulative release observed in the BSA-containing system without invoking micelle destabilization, which is unlikely given the previously demonstrated stability of PEO-*b*-PCL-based micelles in BSA-containing media (Binkhathlan et al., 2024; Forrest et al., 2006).

The stability evaluation of rapamycin-loaded micelles revealed notable differences between the two formulations. While drug retention in PEO_{2000}-*b*-PCL_{4000} micelles declined below 90 % within 1–3 months of storage at 4 °C, the PEO_{2000}-*b*-PCL_{4000}-α-TS micelles maintained % drug retention above 90 % throughout the entire 6-month study period (Fig. 9). This finding suggests that α-TS conjugation may enhance the physical stability of the micellar system, likely through improved structural integrity or interactions with the encapsulated drug.

However, an increase in the PDI of PEO_{2000}-*b*-PCL_{4000}-α-TS micelles was observed over time, ranging from 0.3 to 0.6. This trend may indicate progressive micelle aggregation during storage. While drug retention remained unaffected, such physicochemical changes could potentially influence *in vivo* performance and warrant further investigation. To further explore this aspect, the stability of rapamycin-loaded PEO_{2000}-*b*-PCL_{4000}-α-TS micelles was further assessed under physiological and stress-mimicking conditions by incubating the formulation in various media at 37 °C for 72 h. The micelles remained stable in phosphate-buffered solutions (pH 5.0 and 7.4) and DMEM, showing negligible changes in particle size and PDI (Fig. S5). In contrast, a statistically significant increase in both particle size (from ~29 to ~39 nm) and PDI (from ~0.10 to ~0.28) was observed in normal saline at 72 h ($p < 0.05$) (Fig. S5c). This instability in normal saline may be attributed to its high ionic strength, which can disrupt the PEG–water interactions within the micelles *via* a salting-out effect and promote intermicellar associations, ultimately leading to micelle aggregation. However, these proposed mechanisms remain speculative and require further experimental validation, which will be pursued in future studies.

The results of the *in vitro* cytotoxicity study demonstrate the potential of rapamycin-loaded PEO_{2000}-*b*-PCL_{4000}-α-TS and rapamycin-loaded PEO_{2000}-*b*-PCL_{4000} micelles as effective anti-cancer nanocarriers. Even after 72 h incubation, unloaded micelles exhibited minimal cytotoxicity against normal human fibroblast cells (HFF1), with cell viability remaining above 70 % at concentrations equivalent to those used in 50 μM micellar rapamycin.

In cancer cell lines (A549 and HCT116), rapamycin-loaded micelles demonstrated time-dependent cytotoxic effects (Fig. 10). For HCT116 cells, the PEO_{2000}-*b*-PCL_{4000}-α-TS micelles achieved lower IC_{50} values compared to the unmodified micelles (24.29 μM *vs.* 27.19 μM at 72 h). However, in A549 cells, PEO_{2000}-*b*-PCL_{4000}-α-TS micelles achieved higher IC_{50} values compared to the unmodified micelles (29.51 μM *vs.* 9.18 μM at 72 h) as shown in Table 3. Interestingly, the unloaded micelles also exhibited mild cytotoxic effects against cancer cells (Fig. 10). Similar observations were reported by Bernabeu et al., who demonstrated that unloaded PEO-*b*-PCL and TPGS-*b*-PCL nanoparticles exerted cytotoxic effects on two breast cancer cell lines, MCF-7 and MDA-MB231 (Bernabeu et al., 2016). The exact mechanism underlying this cytotoxicity remains unclear; however, it is generally influenced by several factors, including particle size, concentration, and chemical composition

(Zhang et al., 2012). One possible explanation is that the micelles may have induced cellular stress responses. Nevertheless, further investigations are required to elucidate the underlying mechanisms responsible for this effect.

Taken together, encapsulation within PEO_{2000}-*b*-PCL_{4000}-α-TS and PEO_{2000}-*b*-PCL_{4000} not only enhanced the solubility and provided sustained release of rapamycin but also was effective against cancer cells while sparing the normal cells. However, further investigations involving additional healthy and cancer cell lines, as well as mechanistic studies, are needed to validate and expand upon these findings.

5. Conclusion

This study presents the synthesis and characterization of a novel series of PEO-*b*-PCL-α-TS copolymers and evaluation of their self-assembled micelles as a potential delivery system for rapamycin. The conjugation of α-TS improved drug encapsulation efficiency, solubility, and stability while offering sustained release and effective cytotoxicity against cancer cells. *In vitro* studies also demonstrated that the α-TS-conjugated micelles protected rapamycin from degradation. These findings suggest that PEO-*b*-PCL-α-TS micelles are a promising platform for the delivery of hydrophobic anticancer drugs like rapamycin, combining the benefits of enhanced solubility, stability, sustained drug release, and effective anticancer activity. Future studies focusing on *in vivo* pharmacokinetics and therapeutic efficacy will further validate the clinical potential of this nanocarrier system.

CRediT authorship contribution statement

Ziyad Binkhathlan: Writing – review & editing, Writing – original draft, Visualization, Supervision, Project administration, Methodology, Funding acquisition, Formal analysis, Conceptualization. **Abdullah K. Alshememry:** Project administration, Funding acquisition, Conceptualization. **Ahmad M. Balkhair:** Visualization, Methodology, Investigation, Funding acquisition, Formal analysis. **Raisuddin Ali:** Writing – original draft, Visualization, Methodology, Investigation, Formal analysis. **Sulaiman S. Alhudaithi:** Writing – review & editing, Visualization, Investigation, Formal analysis. **Saad Alobid:** Investigation, Formal analysis. **Wajhul Qamar:** Investigation, Formal analysis. **Alhassan H. Aodah:** Investigation. **Mohammad Reza Vakili:** Writing – review & editing, Methodology, Conceptualization. **Afsaneh Lavasanifar:** Writing – review & editing, Methodology, Conceptualization.

Funding

This work was supported by the Saudi National Institute of Health (Saudi NIH) Grant No. [SNIH-RO-HRT01–2302-KSU-36604592].

Declaration of competing interest

The authors declare that they have no known competing financial interests or personal relationships that could have appeared to influence the work reported in this paper.

Appendix A. Supplementary data

Supplementary data to this article can be found online at https://doi.org/10.1016/j.ijpx.2025.100341.

Data availability

All data presented in this study are available upon request from the corresponding author.

References

Ali, R., Farah, A., Binkhathlan, Z., 2017. Development and characterization of methoxy poly(ethylene oxide)-block-poly(epsilon-caprolactone) (PEO-b-PCL) micelles as vehicles for the solubilization and delivery of tacrolimus. Saudi Pharm. J. 25, 258–265. https://doi.org/10.1016/j.jsps.2016.06.009.

Aliabadi, H.M., Lavasanifar, A., 2006. Polymeric micelles for drug delivery. Expert Opin. Drug Deliv. 3, 139–162. https://doi.org/10.1517/17425247.3.1.139.

Aliabadi, H.M., Mahmud, A., Sharifabadi, A.D., Lavasanifar, A., 2005. Micelles of methoxy poly(ethylene oxide)-b-poly(ε-caprolactone) as vehicles for the solubilization and controlled delivery of cyclosporine a. J. Control. Release 104, 301–311. https://doi.org/10.1016/j.jconrel.2005.02.015.

Baek, N., Lee, J., Park, K., 2004. Aqueous N,N-diethylnicotinamide (DENA) solution as a medium for accelerated release study of paclitaxel. J. Biomater. Sci. Polym. Ed. 15, 527–542. https://doi.org/10.1163/156856204323005343.

Bernabeu, E., Gonzalez, L., Legaspi, M.J., Moretton, M.A., Chiappetta, D.A., 2016. Paclitaxel-loaded TPGS-b-PCL nanoparticles: in vitro cytotoxicity and cellular uptake in MCF-7 and MDA-MB-231 cells versus mPEG-b-PCL nanoparticles and abraxane (R). J. Nanosci. Nanotechnol. 16, 160–170. https://doi.org/10.1166/jnn.2016.10739.

Binkhathlan, Z., Yusuf, O., Ali, R., Alomrani, A.H., Alshamsan, A., Alshememry, A.K., Almomen, A., Alkholief, M., Aljuffali, I.A., Alqahtani, F., Alobid, S., Ali, E.A., Lavasanifar, A., 2024. Polycaprolactone - Vitamin E TPGS micelles for delivery of paclitaxel: in vitro and in vivo evaluation. Int. J. Pharm. X 7, 100253. https://doi.org/10.1016/j.ijpx.2024.100253.

Chang, G.R., Chiu, Y.S., Wu, Y.Y., Chen, W.Y., Liao, J.W., Chao, T.H., Mao, F.C., 2009. Rapamycin protects against high fat diet-induced obesity in C57BL/6J mice. J. Pharmacol. Sci. 109, 496–503. https://doi.org/10.1254/jphs.08215fp.

Chidambaram, M., Manavalan, R., Kathiresan, K., 2011. Nanotherapeutics to overcome conventional cancer chemotherapy limitations. J. Pharm. Pharm. Sci. 14, 67–77. https://doi.org/10.18433/j30c7d.

Dowling, R.J., Topisirovic, I., Fonseca, B.D., Sonenberg, N., 2010. Dissecting the role of mTOR: lessons from mTOR inhibitors. Biochim. Biophys. Acta 1804, 433–439. https://doi.org/10.1016/j.bbapap.2009.12.001.

Forrest, M.L., Won, C.Y., Malick, A.W., Kwon, G.S., 2006. In vitro release of the mTOR inhibitor rapamycin from poly(ethylene glycol)-b-poly(epsilon-caprolactone) micelles. J. Controll. Release 110, 370–377. https://doi.org/10.1016/j.jconrel.2005.10.008.

Geng, Y., Discher, D.E., 2005. Hydrolytic degradation of poly(ethylene oxide)-block-polycaprolactone worm micelles. J. Am. Chem. Soc. 127, 12780–12781. https://doi.org/10.1021/ja053902e.

Grossen, P., Witzigmann, D., Sieber, S., Huwyler, J., 2017. PEG-PCL-based nanomedicines: a biodegradable drug delivery system and its application. J. Controll. Release 260, 46–60. https://doi.org/10.1016/j.jconrel.2017.05.028.

Haeri, A., Osouli, M., Bayat, F., Alavi, S., Dadashzadeh, S., 2018. Nanomedicine approaches for sirolimus delivery: a review of pharmaceutical properties and preclinical studies. Artif. Cells Nanomed. Biotechnol. 46, 1–14. https://doi.org/10.1080/21691401.2017.1408123.

Hartford, C.M., Ratain, M.J., 2007. Rapamycin: something old, something new, sometimes borrowed and now renewed. Clin. Pharmacol. Ther. 82, 381–388. https://doi.org/10.1038/sj.clpt.6100317.

Kim, M.S., Kim, J.S., Cho, W.K., Hwang, S.J., 2013. Enhanced solubility and oral absorption of sirolimus using D-alpha-tocopheryl polyethylene glycol succinate micelles. Artif. Cells Nanomed. Biotechnol. 41, 85–91. https://doi.org/10.3109/21691401.2012.742100.

Krebs, M., Brunmair, B., Brehm, A., Artwohl, M., Szendroedi, J., Nowotny, P., Roth, E., Furnsinn, C., Promintzer, M., Anderwald, C., Bischof, M., Roden, M., 2007. The Mammalian target of rapamycin pathway regulates nutrient-sensitive glucose uptake in man. Diabetes 56, 1600–1607. https://doi.org/10.2337/db06-1016.

Lampen, A., Zhang, Y., Hackbarth, I., Benet, L.Z., Sewing, K.-F., Christians, U., 1998. Metabolism and transport of the macrolide immunosuppressant sirolimus in the small intestine. J. Pharmacol. Exp. Ther. 285, 1104–1112. https://doi.org/10.1016/s0022-3565(24)37526-3.

Law, B.K., 2005. Rapamycin: an anti-cancer immunosuppressant? Crit. Rev. Oncol. Hematol. 56, 47–60. https://doi.org/10.1016/j.critrevonc.2004.09.009.

Lee, J., Lee, S.C., Acharya, G., Chang, C.J., Park, K., 2003. Hydrotropic solubilization of paclitaxel: analysis of chemical structures for hydrotropic property. Pharm. Res. 20, 1022–1030. https://doi.org/10.1023/a:1024458206032.

Li, J., Kim, S.G., Blenis, J., 2014. Rapamycin: one drug, many effects. Cell Metab. 19, 373–379. https://doi.org/10.1016/j.cmet.2014.01.001.

Lin, W.J., Wang, C.L., Chen, Y.C., 2005. Comparison of two pegylated copolymeric micelles and their potential as drug carriers. Drug Deliv. 12, 223–227. https://doi.org/10.1080/10717540590952672.

Lipinski, C., 2002. Poor aqueous solubility - an industry wide problem in drug discovery. Am. Pharm. Rev. 5, 82–85.

MacDonald, A., Scarola, J., Burke, J.T., Zimmerman, J.J., 2000. Clinical pharmacokinetics and therapeutic drug monitoring of sirolimus. Clin. Ther. 22 (Suppl B), B101–B121. https://doi.org/10.1016/s0149-2918(00)89027-x.

Merciadez, M., Alquier, L., Mehta, R., Patel, A.J., Wang, A., 2011. A novel method for the elution of sirolimus (rapamycin) in drug-eluting stents. Dissolut. Technol. 18, 37–42.

Neuzil, J., Weber, T., Gellert, N., Weber, C., 2001. Selective cancer cell killing by alpha-tocopheryl succinate. Br. J. Cancer 84, 87–89. https://doi.org/10.1054/bjoc.2000.1559.

Ong, P.S., Wang, L.Z., Dai, X., Tseng, S.H., Loo, S.J., Sethi, G., 2016. Judicious toggling of mTOR activity to combat insulin resistance and cancer: current evidence and perspectives. Front. Pharmacol. 7, 395. https://doi.org/10.3389/fphar.2016.00395.

Othman, R., Vladisavljevic, G.T., Nagy, Z.K., Holdich, R.G., 2016. Encapsulation and controlled release of rapamycin from polycaprolactone nanoparticles prepared by membrane micromixing combined with antisolvent precipitation. Langmuir 32, 10685–10693. https://doi.org/10.1021/acs.langmuir.6b03178.

Otsuka, H., Nagasaki, Y., Kataoka, K., 2003. PEGylated nanoparticles for biological and pharmaceutical applications. Adv. Drug Deliv. Rev. 55, 403–419. https://doi.org/10.1016/s0169-409x(02)00226-0.

Oyler, A.R., Segmuller, B.E., Sun, Y., Polshyna, A., Dunphy, R., Armstrong, B.L., Achord, P., Maryanoff, C.A., Alquier, L., Il'ichev, Y.V., 2012. Forced degradation studies of rapamycin: identification of autoxidation products. J. Pharm. Biomed. Anal. 59, 194–200. https://doi.org/10.1016/j.jpba.2011.10.017.

Prasad, K.N., Edwards-Prasad, J., 1982. Effects of tocopherol (vitamin E) acid succinate on morphological alterations and growth inhibition in melanoma cells in culture. Cancer Res. 42, 550–555.

Prasad, K.N., Kumar, B., Yan, X.D., Hanson, A.J., Cole, W.C., 2003. Alpha-tocopheryl succinate, the most effective form of vitamin E for adjuvant cancer treatment: a review. J. Am. Coll. Nutr. 22, 108–117. https://doi.org/10.1080/07315724.2003.10719283.

Sehgal, S.N., Baker, H., Vezina, C., 1975. Rapamycin (AY-22,989), a new antifungal antibiotic. II. Fermentation, isolation and characterization. J. Antibiot. (Tokyo) 28, 727–732. https://doi.org/10.7164/antibiotics.28.727.

Simamora, P., Alvarez, J.M., Yalkowsky, S.H., 2001. Solubilization of rapamycin. Int. J. Pharm. 213, 25–29. https://doi.org/10.1016/s0378-5173(00)00617-7.

Sylvester, P.W., 2007. Vitamin E and Apoptosis, Vitamins & Hormones. Academic Press, pp. 329–356.

Theerasilp, M., Nasongkla, N., 2013. Comparative studies of poly(epsilon-caprolactone) and poly(D,L-lactide) as core materials of polymeric micelles. J. Microencapsul. 30, 390–397. https://doi.org/10.3109/02652048.2012.746746.

Trepanier, D.J., Gallant, H., Legatt, D.F., Yatscoff, R.W., 1998. Rapamycin: distribution, pharmacokinetics and therapeutic range investigations: an update. Clin. Biochem. 31, 345–351. https://doi.org/10.1016/s0009-9120(98)00048-4.

Turley, J.M., Funakoshi, S., Ruscetti, F.W., Kasper, J., Murphy, W.J., Longo, D.L., Birchenall-Roberts, M.C., 1995. Growth inhibition and apoptosis of RL human B lymphoma cells by vitamin E succinate and retinoic acid: role for transforming growth factor beta. Cell Growth Differ. 6, 655–663.

Turley, J.M., Fu, T., Ruscetti, F.W., Mikovits, J.A., Bertolette 3rd, D.C., Birchenall-Roberts, M.C., 1997. Vitamin E succinate induces Fas-mediated apoptosis in estrogen receptor-negative human breast cancer cells. Cancer Res. 57, 881–890.

Um, S.H., Frigerio, F., Watanabe, M., Picard, F., Joaquin, M., Sticker, M., Fumagalli, S., Allegrini, P.R., Kozma, S.C., Auwerx, J., Thomas, G., 2004. Absence of S6K1 protects against age- and diet-induced obesity while enhancing insulin sensitivity. Nature 431, 200–205. https://doi.org/10.1038/nature02866.

van der Wagt, M.A.J., Touw, D.J., Dekkers, B.G.J., 2024. Poor solubility and stability of rapamycin in aqueous environments. Biomed. Pharmacother. 176, 116865. https://doi.org/10.1016/j.biopha.2024.116865.

van Meerloo, J., Kaspers, G.J., Cloos, J., 2011. Cell sensitivity assays: the MTT assay. Methods Mol. Biol. 731, 237–245. https://doi.org/10.1007/978-1-61779-080-5_20.

Wagner, A.J., Ravi, V., Riedel, R.F., Ganjoo, K., Van Tine, B.A., Chugh, R., Cranmer, L., Gordon, E.M., Hornick, J.L., Du, H., Grigorian, B., Schmid, A.N., Hou, S., Harris, K., Kwiatkowski, D.J., Desai, N.P., Dickson, M.A., 2021. Nab-sirolimus for patients with malignant perivascular epithelioid cell tumors. J. Clin. Oncol. 39, 3660–3670. https://doi.org/10.1200/JCO.21.01728.

Weber, T., Lu, M., Andera, L., Lahm, H., Gellert, N., Fariss, M.W., Korinek, V., Sattler, W., Ucker, D.S., Terman, A., Schroder, A., Erl, W., Brunk, U.T., Coffey, R.J., Weber, C., Neuzil, J., 2002. Vitamin E succinate is a potent novel antineoplastic agent with high selectivity and cooperativity with tumor necrosis factor-related apoptosis-inducing ligand (Apo2 ligand) in vivo. Clin. Cancer Res. 8, 863–869.

Woodruff, M.A., Hutmacher, D.W., 2010. The return of a forgotten polymer—polycaprolactone in the 21st century. Prog. Polym. Sci. 35, 1217–1256. https://doi.org/10.1016/j.progpolymsci.2010.04.002.

Yalkowsky, S.H., 1999. Solubility and Solubilization in Aqueous Media.

Yanez, J.A., Forrest, M.L., Ohgami, Y., Kwon, G.S., Davies, N.M., 2008. Pharmacometrics and delivery of novel nanoformulated PEG-b-poly(epsilon-caprolactone) micelles of rapamycin. Cancer Chemother. Pharmacol. 61, 133–144. https://doi.org/10.1007/s00280-007-0458-z.

Yu, W., Heim, K., Qian, M., Simmons-Menchaca, M., Sanders, B.G., Kline, K., 1997. Evidence for role of transforming growth factor-beta in RRR-alpha-tocopheryl succinate-induced apoptosis of human MDA-MB-435 breast cancer cells. Nutr. Cancer 27, 267–278. https://doi.org/10.1080/01635589709514537.

Zhang, X.Q., Xu, X., Bertrand, N., Pridgen, E., Swami, A., Farokhzad, O.C., 2012. Interactions of nanomaterials and biological systems: implications to personalized nanomedicine. Adv. Drug Deliv. Rev. 64, 1363–1384. https://doi.org/10.1016/j.addr.2012.08.005.

Zweers, M.L., Engbers, G.H., Grijpma, D.W., Feijen, J., 2004. In vitro degradation of nanoparticles prepared from polymers based on DL-lactide, glycolide and poly (ethylene oxide). J. Controll. Release 100, 347–356. https://doi.org/10.1016/j.jconrel.2004.09.008.